



Research article

Design, synthesis, *in-silico* studies and apoptotic activity of novel amide enriched 2-(1*H*)-quinazolinone derivativesNaganjaneyulu Gariganti^{a,b}, Anjaneyulu Bandi^c, K.R.S. Naresh Gatta^c, Jishu Pagag^c, Lalitha Guruprasad^c, Bhaskar Poola^b, Ravi K. Kottalanka^{a,*}^a Department of Chemistry, School of Applied Science and Humanities, Vignan's Foundation for Science Technology and Research, Vadlamudi, Guntur, Andhra Pradesh, 522213, India^b Neuland Laboratories Ltd., Hyderabad, Telangana, 500034, India^c School of Chemistry, University of Hyderabad, Gachibowli, Hyderabad, 500046, India

ARTICLE INFO

Keywords:

Quinazolinone
Apoptotic activity
SARS studies
Molecular docking
MD simulations
ADME analysis
DFT studies

ABSTRACT

Cancer is a broad classification of diseases that can affect any organ or body tissue due to aberrant cellular proliferation for unknown reasons. Many present chemotherapeutic drugs are highly toxic and have little selectivity. Additionally, they lead to the development of medication resistance. Therefore, developing tailored chemotherapeutic drugs with minimal side effects and good selectivity is crucial for cancer treatment. 2-(1*H*)-Quinazolinone is one of the vital scaffold and anticancer activity is one of the prominent biological activities of this class. Here we report the novel set of amide-enriched 2-(1*H*)-quinazolinone derivatives (**7a-j**) and their apoptotic activity with the help of MTT assay method against four human cancer cell lines: PC3 (prostate cancer), DU-145 (prostate cancer), A549 (lung cancer), and MCF7 (breast cancer). When compared to etoposide, every synthetic test compound (**7a-j**) exhibited moderate to excellent activity. The IC₅₀ values of the new amide derivatives (**7a-j**) varied from 0.07 ± 0.0061 μM to 10.8 ± 0.69 μM. While the positive control, etoposide, exhibited 1.97 ± 0.45 μM to 3.08 ± 0.135 μM range. Among the novel amide derivatives (**7a-j**), in particular, **7i** and **7j** showed strong apoptotic activity against MCF7; **7h** showed against PC3, and **7g** showed against DU-145. Molecular docking studies of test compounds (**7a-j**) with the EGFR tyrosine kinase domain (PDB ID: 1M17) protein provided the significant docking scores for each test compound (**7a-j**) (−9.00 to −9.67 kcal/mol). Additionally, DFT investigations and MD simulations validated the predictions of molecular docking. According to the findings of the ADME analysis, oral absorption by humans is anticipated to be higher than 85 % for all test compounds.

1. Introduction

Cancer is a severe problem in both developed and underdeveloped countries. According to the International Agency for Research on Cancer (IARC), one in every five people will develop cancer at some point in their lives [1–3]. The most common types of cancer are breast, lung, prostate, and colon cancer. Invasive procedures such as surgery and hazardous medication such as chemotherapy and radiotherapy are most common treatments. These procedures have downsides, such as the careless destruction of healthy cells and the

* Corresponding author.

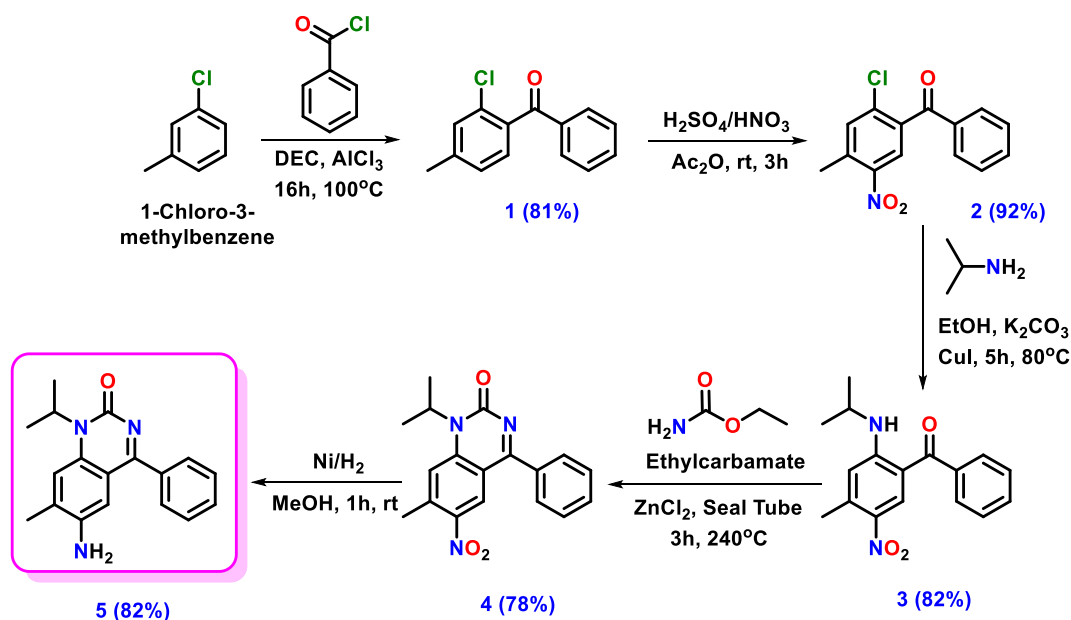
E-mail addresses: drkrk_sh@vignan.ac.in, ravikottalanka@gmail.com (R.K. Kottalanka).<https://doi.org/10.1016/j.heliyon.2024.e30292>

Received 14 November 2023; Received in revised form 22 April 2024; Accepted 23 April 2024

Available online 26 April 2024

2405-8440/© 2024 The Author(s). Published by Elsevier Ltd. This is an open access article under the CC BY-NC license (<http://creativecommons.org/licenses/by-nc/4.0/>).

development of medication resistance etc. [4,5] Therefore, developing tailored chemotherapeutic drugs with minimal side effects and good selectivity is crucial for cancer treatment. Heterocyclic compounds are key synthetic targets for the creation of new chemotherapeutics with good selectivity and are being studied extensively as bioactive molecules [6–15]. Quinazolines are well-studied phenyl pyrimidine heterocycles with potential biological applications [16,17]. The quinazoline moiety serves as a fundamental structural unit in various physiologically active chemicals and medicinal molecules [18]. Quinazoline and quinazolinone derivatives have been attracted by biologists and medicinal chemists due to their diverse pharmacological activities [19,20], including anticancer [21–24], antitubercular [25–27], antimalarial [28], anti-inflammatory [29,30], antimicrobial [31], anticonvulsant [32], antihypertensive [33,34], antidiabetic [35], anti-HIV [36], antitumor [37–39], antioxidant [40], antiviral [41], kinase inhibitory [42], sedative-hypnotic, antihistaminic and many other uses [43]. Quinazoline and its derivatives are promising cancer chemotherapeutic agents for treating solid tumors [44–50]. The FDA has approved many quinazoline derivatives for clinical use as cancer treatments. These drugs include Erlotinib, Afatinib, Imatinib, Gefitinib, Lapatinib, Vandetanib and Lcotinib [51,52]. However, fewer number of anticancer agents were reported, where 2-quinazolinone (quinazolin-2(1H)-one) is basic structural unit [53]. As a part of our ongoing research towards the design and development of bioactive anticancer drug molecules, we designed the series of novel quinazolinone-based molecules by introducing isopropyl group at 1st position (at amine nitrogen center) and phenyl group at 4th position of phenyl pyrimidine 2-quinazolinone (at imine nitrogen center) and tunable amide functionality at 6th position of the phenyl pyrimidine 2-quinazolinone structural unit. Molecular modeling studies predicted that substituent modification at amide functionality of phenyl pyrimidine 2-quinazolinone unit will produce potential anticancer agents that can bind with several enzymes, including epidermal growth factor receptor (EGFR), dihydrofolate reductase, folate thymidylate synthase, tyrosine kinase, aldose reductase, cyclic GMP phosphodiesterase, and DNA repairing enzyme [54–56]. The four EGFR subfamilies (erbB-1 to 4) regulate the proliferation, apoptosis evasion, angiogenesis, migration, and metastasis of cancer cells. Breast, lung, colon, and bladder cancers, as well as other solid tumors with unfavorable prognoses, are brought on by the overexpression of EGFR [30]. We have therefore selected EGFR tyrosine kinase domain (EGFR TKD) as drug targets implicated in breast, lung and prostate cancers. Here we proposed 26 novel quinazolinone derivatives (7a-z) by altering the substitution at position “C6” will affect molecules biological activity (Chart-S1 in SI). All 26 novel quinazolinone derivatives designed were investigated for their possible biological significance by using molecular docking studies to better understand the structure-activity correlation. Non-covalent interactions such as H-bonds, pi-stacking, ionic and van der Waals interactions are involved when a drug molecule binds with protein targets. The molecular docking scores of all the proposed quinazolinone derivatives (7a-z) and the reference molecules such as Etoposide and Erlotinib were provided in Table S1 in SI. Further, the pharmacokinetic characteristics of all the proposed quinazolinone derivatives and reference molecules were also investigated and provided in Table S2 in SI. After preliminary screening of all proposed quinazolinone derivatives by computer-aided methods, quinazolin-2-(1H)-one derivatives (7a-j) were selected and synthesized in our research lab by utilizing novel synthetic methodology and easily accessible starting materials. All of the synthesized quinazolin-2-(1H)-one derivatives (7a-j) were fully characterized and their structures validated utilizing spectroscopic/analytical techniques such as NMR spectroscopy and mass spectrometry. Furthermore, utilizing HPLC analysis to determine the purity of each derivative (7a-j), it was observed that all tested compounds had a purity of at least 95%. *In-vitro* cytotoxicity of all the synthesized quinazolin-2-(1H)-one derivatives (7a-j) were investigated by using the MTT assay method against the four human cancer cell lines MCF7 (Breast cancer), A549 (Lung cancer), PC3 (Prostate cancer) and DU-145 (Prostate cancer) and Etoposide is used as a positive control. Among all quinazolin-2-(1H)-one scaffolds tested, the test compounds 7a



Scheme 1. Synthesis of 6-amino-1-isopropyl-7-methyl-4-phenylquinazolin-2(1H)-one (5).

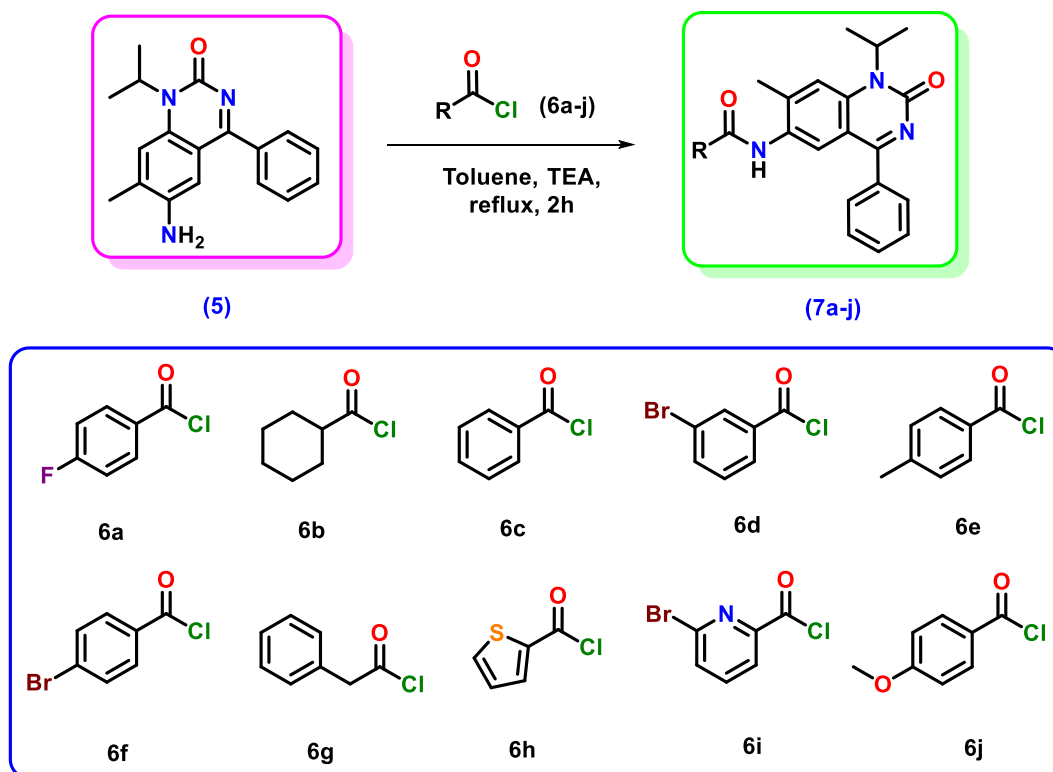
and **7c** demonstrated modest activity with reference to “Etoposide,” while **7g-j** showed exceptional cytotoxicity against four human cancer cell lines. Particularly, **7h**, **7i**, and **7j** showed remarkable activity against all four human cancer cell lines. The results from *in silico* molecular docking studies by using EGFR tyrosine kinase domain (EGFR TKD) (1M17), as protein target are consistent with the experimentally derived results for quinazolinone derivatives (**7a-j**). The docking scores of the newly produced quinazolinone derivatives (**7a-j**) with EGFR tyrosine kinase domain (EGFR TKD) (1M17) protein target varied from -9.00 kcal/mol to -9.67 kcal/mol whereas reference standard etoposide showed docking score as -7.66 kcal/mol, indicating that, the proposed 2-quinazolinone derivatives (**7a-j**) have reasonably good binding affinities with the protein target compared to etoposide. However, the real-time biological activity under *in-vitro* or *in-vivo* conditions may differ from molecular docking predictions. Molecular docking predictions were further supported by MD simulations and DFT studies. According to the findings of the ADME analysis, oral absorption by humans is anticipated to be higher than 85 % for all test compounds.

2. Results and discussion

2.1. Synthesis of 6-amino-1-isopropyl-7-methyl-4-phenylquinazolin-2(1H)-one (**5**)

A new series of amide enriched 2-(1H)-quinazolinone derivatives (**7a-j**) derived from 6-amino 1isopropyl-7-methyl-4-phenylquinazolin-2(1H)-one (**5**) has been synthesized in a traditional step by-step synthetic methodology as described in Schemes 1 and 2 with good to moderate yields in every step. Friedel-Crafts acetylation of 1-chloro-3-methyl benzene with benzoyl chloride in presence of AlCl_3 offered (2-chloro-4-methylphenyl) (phenyl)methanone (**1**, 51 %) and 4-chloro-2- methylphenyl) (phenyl)methanone (35 %). The intermediate (2-chloro-4-methylphenyl) (phenyl)methanone (**1**) was further subjected to nitration in the presence of $\text{H}_2\text{SO}_4/\text{HNO}_3$ and acetic anhydride to get 2-chloro-4-methyl-5-nitrophenyl)(phenyl)methanone (**2**), as another key intermediate with good yield (92 %). Further, treatment of intermediate compound **2** with isopropyl amine in the presence of K_2CO_3 and CuI offered the 2-chloro-4-methyl-5-nitrophenyl) (phenyl)methanone (**3**) with 82 % yield. The reaction of compound **3** with ethyl-carbamate in the presence of ZnCl_2 at 240°C in a sealed tube offered 1-isopropyl-7-methyl-6-nitro-4-phenylquinazolin-2(1H)-one (**4**) with 78 % yield. Finally, the nitro group of the intermediate compound (**4**) reduced to amine functionality with the help of Raney Ni, H_2 gas in methanol solvent afforded the desired amine compound such as 6-amino-1-isopropyl-7-methyl-4-phenylquinazolin-2(1H)-one (**5**) with 82 % yield.

All the intermediate compounds (**1-5**) were characterized by using spectroscopic/analytical techniques and corresponding data was given in the experimental section and spectral data was presented in supporting information. The structurally characterized key intermediate compound (**5**) is then further treated with various aryl acid chlorides (**6a-j**) to achieve the target amine enriched 2-(1H)-



Scheme 2. Synthesis of target amide enriched 2-(1H)-quinazolinone derivatives (**7a-j**).

quinazolinone derivatives (**7a-j**) in the presence of triethylamine as a base in toluene solvent under reflux condition as shown in [Scheme 2](#). The final amide derivatives (**7a-j**) derived from 6-amino-1-isopropyl-7-methyl-4-phenylquinazolin-2(1H)-one (**5**) was fully characterized by spectroscopic/analytical techniques.

2.2. Biological evaluation

2.2.1. In-vitro cytotoxicity

The newly synthesized amide enriched 2-(1H)-quinazolinone derivatives (**7a-j**) were examined for their *in-vitro* cytotoxicity against four human cancer cell lines such as MCF7 (Breast cancer), A549 (Lung cancer), PC3 (prostate cancer) and DU-145 (Prostate cancer) by using the MTT assay and obtained results i.e., the half maximal inhibitory concentration (IC₅₀) of the tested compounds on the four human cancer cell lines are summarized and reported in [Table 1](#). The chemotherapeutic anticancer drug such as etoposide is used as positive control. Most of the tested compounds displayed excellent-good and good-moderate activities compared to etoposide under *in-vitro* conditions. This could be presumably due to the enhanced lipophilic nature of the incorporated tunable amide functionality and appended quinazolinone system in **7a-j** compounds. The IC₅₀ values of the novel amide derivatives (**7a-j**) ranged from 0.07 ± 0.0061 μM to 10.8 ± 0.69 μM whereas positive control (Etoposide) showed 1.97 ± 0.45 μM to 3.08 ± 0.135 μM, for all the human cancer cell lines studied. The developed quinazolinone derivatives of 6-amino-1-isopropyl-7-methyl-4-phenylquinazolin-2(1H)-one was found to have significant biological impact and they can be transformed to good cytotoxic agents after in-depth analysis and clinical trials at the later stages. The present study i.e. MTT assay investigations predicted that apoptotic activity of the test compounds (**7a-j**) under *in-vitro* conditions. Among the new amide derivatives (**7a-j**), particularly **7g-j** displayed highly potent apoptotic activity towards MCF7 (**7i**, **7j**), PC3 (**7h**), and DU-145 (**7g**) human cancer cell lines respectively. Among the investigated compounds, four compounds (**7g**, **7h**, **7i**, and **7j**) displayed potent apoptotic activities at all investigating doses (See [Table 1](#)).

It was observed that compound **7i** with heterocyclic ring(6-bromopicolinoyl) substitution linked to amide functionality showed excellent apoptotic activity, which can be evident by IC₅₀ values (Entry 9 in [Table 1](#)), on four used human cancer cell lines, as MCF-7 = 0.07 ± 0.0061 μM; A549 = 0.19 ± 0.045 μM; PC3 = 0.012 ± 0.021 μM and DU-145 = 1.64 ± 0.12 μM compared to etoposide (Entry 11). Also, the compound **7j** with electron-rich segment (4-methoxy) group as a substituent on the phenyl ring linked to amide functionality displayed excellent apoptotic activity on MCF-7 = 0.13 ± 0.053 μM; A549 = 1.23 ± 0.19 μM; PC3 = 1.81 ± 0.22 μM and DU-145 = 1.63 ± 0.11 μM compared to etoposide (Entry 11); Compound **7h** with heterocyclic ring (thiophene) substitution linked to amide functionality showed good apoptotic activity on four human cancer cell lines MCF-7 = 1.85 ± 0.14 μM; A549 = 1.27 ± 0.03 μM; PC3 = 0.77 ± 0.086 μM and DU-145 = 1.02 ± 0.065 μM compared to etoposide (Entry 11) and compound **7g** with heterocyclic ring (benzyl) substitution showed good apoptotic activity on four human cancer cell lines MCF7 = 2.29 ± 0.41 μM; A549 = 2.11 ± 0.28 μM; PC3 = 2.09 ± 0.17 μM and DU-145 = 1.98 ± 0.27 μM compared to etoposide (Entry 11) and showed slightly lower activity when compared with compound **7j** (see Entries 7 and 10). However, as expected compound **7b** (Phenyl), **7c** (cyclohexyl), and **7e** (Methyl benzyl) substitution on phenyl ring linked to amide functionality displayed relatively lower activity compared to **7h** and etoposide (Entry 8 & 11) due to the reduced inductive effect. The remaining test compounds with electron-withdrawing substituents **7a** (4-fluorophenyl), **7d** (3-bromobenzoyl) and **7f** (4-bromophenylacetyl) substitution showed weak apoptotic activity when compared with etoposide (see entry 1, 4, 6 and 11) due to presence of electron-withdrawing groups on aryl substitution, which further influences the binding capacity of amide (-C(=O)-NH) group during the interactions with drug targets of various human cancer cell lines. These results suggested that the designed quinazolin-2-one derivatives having 6-amino-1-isopropyl-7-methyl-4-phenylquinazolin-2(1H)-one (**7a-j**) are promising candidates for future cytotoxic molecules discovery.

Table 1

Screening results of apoptotic activity of the test compounds (**7a-j**) expressed as IC₅₀ (μM) using the MTT assay. All the values are expressed as the mean ± SD of triplicate experiments.^a

Entry	Compound	^c MCF-7	^d A549	^e PC3	^f DU-145
1	7a	3.48 ± 0.21	4.11 ± 0.34	ND	ND
2	7b	6.21 ± 0.29	6.43 ± 0.78	5.62 ± 0.51	ND
3	7c	ND	2.91 ± 0.17	4.25 ± 0.33	3.96 ± 0.16
4	7d	7.52 ± 0.33	ND	ND	5.97 ± 0.41
5	7e	ND	10.8 ± 0.69	3.10 ± 0.39	7.44 ± 0.51
6	7f	6.71 ± 0.61	ND	8.24 ± 0.51	7.19 ± 0.54
7	7g	2.29 ± 0.41	2.11 ± 0.28	2.09 ± 0.17	1.98 ± 0.27
8	7h	1.85 ± 0.14	1.27 ± 0.03	0.77 ± 0.086	1.02 ± 0.065
9	7i	0.07 ± 0.0061	0.19 ± 0.045	0.12 ± 0.021	1.64 ± 0.12
10	7j	0.13 ± 0.053	1.23 ± 0.19	1.81 ± 0.22	1.63 ± 0.11
11	Etoposide	2.11 ± 0.024	3.08 ± 0.135	2.39 ± 1.56	1.97 ± 0.45

ND = Not deter mi ne.

^a Each data represents as mean ± S. D values. From three different experiments performed in triplicates.

^c MCF-7: human breast cancer cell line.

^d A549: human lung cancer cell line.

^e PC3: human prostate cancer cell line.

^f DU-145: human prostate cancer cell line.

Table 2Molecular docking scores and active interactions of test compounds (**7a-j**) with EGFR TKD (PDB ID: 1M17).

Test compound	Docking score (kcal/mol)	Inhibition Constant, K_i^a (nM/ μ M)	Amino acid residues interacting with reference and test compounds
7a	-9.59	92.70 nM	H-Bond: Arg817(3.64 Å), Met769(2.30 Å) and Asp831(1.91 Å); Hydrophobic: Leu694(3.47 Å), Ala719(3.60 Å), Lys721(3.27 Å), Leu764(3.97 Å), Thr766(3.71 Å), Met769(3.23 Å) and Leu820(3.85 Å)
7b	-9.11	98.16 nM	H-Bond: Thr766(3.67 Å), Met769(2.13 Å) and Asp831(2.11 Å); Hydrophobic: Leu694(3.75 Å), Phe699(3.41, 3.49 & 3.72 Å), Lys721(3.69 Å), Thr766(3.75 Å), Met769(3.09 Å) and Leu820(3.56 Å); π-Stacking: Lys721(5.31 Å)
7c	-9.29	154.67 nM	H-Bond: Thr766(3.70 Å), Met769(2.23 Å) and Asp831(2.19 Å); Hydrophobic: Leu694(3.65 Å), Phe699(3.76 Å), Thr766(3.85 Å), Met769(3.03 Å) and Leu820(3.52 Å); π-Stacking: Phe699(4.05 Å)
7d	-9.17	162.48 nM	H-Bond: Met769(2.13 Å) and Asp831(1.88 Å); Hydrophobic: Leu694(3.70 Å), Phe699(3.80 Å), Lys721(3.69 Å), Thr766(3.59 Å), Met769(3.19 Å) and Leu820(3.28 & 3.44 Å); π-Stacking: Phe699(4.09 Å)
7e	-9.03	239.76 nM	H-Bond: Lys721(2.27 Å) and Asp831(3.41 & 3.40 Å); Hydrophobic: Leu694(3.49 Å), Phe699(3.34 Å), Val702(3.80 Å), Ala719(3.41 Å), Lys721(3.92 Å), and Leu820(3.23 Å)
7f	-9.00	250.54 nM	H-Bond: Lys721(2.30 Å) and Asp831(3.30 & 3.31 Å); Hydrophobic: Leu694(3.37 Å), Phe699(3.63 Å), Val702(3.46 Å), Ala719(3.97 Å), Asp831(3.73 Å), and Leu820(3.18, 3.85 & 3.98 Å)
7g	-9.41	126.35 nM	H-Bond: Thr766(3.64 Å), Met769(2.23 Å) and Asp831(1.90 Å); Hydrophobic: Leu694(3.49 Å), Phe699(3.77 Å), Lys721(3.75 Å), Thr766(3.39 Å), Met769(3.31 Å) and Leu820(3.61 Å)
7h	-9.31	81.63 nM	H-Bond: Met769(2.87 Å) and Asp831(2.94 Å); Hydrophobic: Leu694(3.56 Å), Ala719(3.87 Å), Lys721(3.47 Å), Thr766(3.52 Å), Met769(3.38 Å) and Leu820(3.31 & 3.51 Å); π-Stacking: Phe699(4.17 Å)
7i	-9.67	82.15 nM	H-Bond: Lys721(2.76 Å), Asp831(2.73 Å); Hydrophobic: Ala719(3.17 Å), Met769(3.49 Å), Leu820(3.89 Å) and Asp831(3.55 Å)
7j	-9.65	84.46 nM	H-Bond: Lys721(3.03 Å) and Met769(2.95 Å); Hydrophobic: Leu694(3.35 Å), Val702(3.56 Å), Ala719(3.53 Å), Lys721(3.35 Å), Leu764(3.60 Å), Thr766(3.58 Å), Leu768(3.64 Å), Met769(3.09 Å) and Leu820(3.37 Å); π-Stacking: Phe699(4.48 Å)
Erlotinib	-7.54	2.96 μ M	H-Bond: Cys773(2.24 Å) and Met769(4.15 Å); Hydrophobic: Val702(3.65 Å), Lys721(3.70 Å), Thr766(3.73 Å), Asp831(3.47 Å), Gly772(3.72 Å); π-Cation Interactions: Lys721(4.81 Å)
Etoposide	-7.66	2.41 μ M	H-Bond: Cys773(3.27 Å), and Arg817(2.57 & 3.02 Å); Hydrophobic: Leu820(3.32 Å), Thr830(3.65 Å).

^a Inhibitory constant (K_i) values are generated theoretically from molecular docking methodology.

2.3. Molecular docking studies

The molecular docking studies were used to screen the binding interactions of the investigated test compounds (**7a-j**) utilizing the AutoDock v4.2.6 suite. AutoDock v4.2.6 uses the Lamarckian Genetic Algorithm (LGA) as a search engine to automate docking investigations [54]. The pdbqt files for the receptor and the ligand were prepared using the graphical interface of the auto-docking

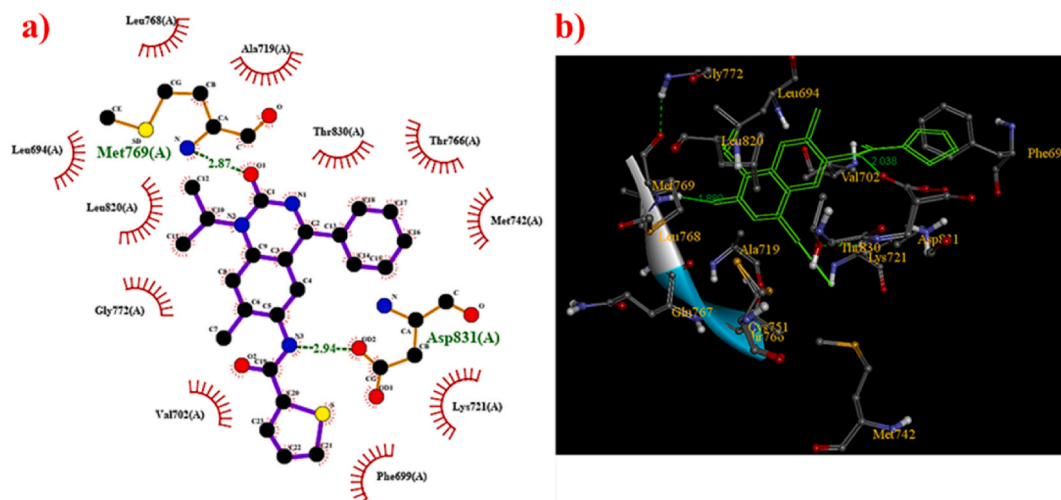


Fig. 1. 2D (left side (a)) and 3D (right side (b)) Docking interaction profiler of **7i** with EGFR-TKD active site of protein(1M17).

application ADT4.2. The 2D structures (7a-j) of the target compounds were sketched in ChemDraw and saved as pdb files. The ligand files were subjected to energy minimization (force field-uff) using the open babel tool and conformers (AutoDock pdbqt files) were then generated in Auto Dock tool. The structure of chosen protein, Epidermal Growth Factor Receptor tyrosine kinase domain (EGFR TKD) with 4-anilinoquinazoline inhibitor erlotinib (1M17) was downloaded from RSCB Protein Data Bank [55,56]. Before docking, the co-crystal ligand i.e., 4-anilinoquinazoline inhibitor (Erlotinib) and the molecular waters were eliminated as per standard docking protocol. The Ramachandran plot was generated using Discovery Studio 4.1 to examine whether amino acid residues reside in “accepted region” or “unaccepted” region. All hydrogens were added, non-polar hydrogens were merged, Kollman charges were added, and missing atoms were added and assigned the AD4 type. The three-dimensional energy scoring grids with a resolution of 0.375 Å and dimensions of 60 Å × 60 Å × 60 Å were computed, and the xyz coordinates of co-crystal (Erlotinib) were extracted from Discovery studio (X = 20.676, Y = 9.289, and Z = 55.459) to generate a grid box around the region where the co-crystal ligand exhibits interactions with amino acid residues in target. The ligands (test compounds) were finally docked at the active sites using the Molecular Docking tool. Docking was done using the LGA default settings. The docked results were subjected to cluster analysis with a RMSD tolerance of 2.0 Å. The Discovery Studio Visualizer tool was used to analyze the binding modes and to understand the intermolecular interactions between the active sites of the target protein and test compounds (7a-j) [57,58]. Before proceeding to the docking analysis of the test compounds (7a-j), the reliability of the docking results was rechecked by redocking a co-crystallized ligand i.e. Erlotinib at the TKD-binding site of EGFR. The active site of EGFR in its TKD-binding domain, allows a small pocket for ligand entry and binding. The site consists of hydrogen bond amino acid residues (Cys773 and Met769), hydrophobic amino acid residues (Val702, Lys721, Thr766, Asp831, Gly772, Leu764, Leu 694), negatively charged residues (Glu738), positively charged residues (Arg817 and Lys721), and polar amino acids (Thr830 and Thr766) (See Fig. S1 in SI). The RMSD between the original and post-docking orientation is found to be 0.325 Å, confirming the methodology’s accuracy. The docking score of the co-crystal i.e. Erlotinib inhibitor is found to be −7.54 kcal/mol and inhibition constant (Ki) was predicted to be 2.96 μM. Once the re-docking results were satisfactory, the test compounds (7a-j) are processed, optimized for protein binding, and the corresponding docking scores were assessed, which shows their viability in binding interactions with the active sites of the target protein. The predicted molecular docking results for test compounds (7a-j) were summarized in Table 2. In addition to test compounds (7a-j), the docking interactions of Etoposide with active site of EGFR-TKD (1M17) were also predicted and the corresponding details were provided in supplementary information (See Fig. S2 in SI) though Etoposide is not best suited for the selected target protein EGFR-TKD (1M17).

The test molecule 7i (6-bromo-N-(1-isopropyl-7-methyl-2-oxo-4-phenyl-1,2-dihydroquinazolin-6-yl)picolinamide) gave the more negative docking score (−9.67 kcal/mol) against the EGFR tyrosine kinase domain (1M17), also demonstrated the exceptional potent inhibitory activity on four human cancer cell lines tested in the MTT assay. Upon analyzing the docking pose of 7i within the EGFR tyrosine kinase domain (1M17) binding site, it was noted that several hydrophobic residues, including Phe699, Val702, Ala719, Met769, Leu820, Leu768, Gln767, Gly772, Thr830, and Thr766, surround the supplied ligand, or test compound 7i. The EGFR-TKD protein target (1M17) and the test compound 7i are found to bind through a donor type H-bond between nitrogen of its amide group and Asp831, neighboring polar Lys721 residue, through pi-sulfates interaction of Met742 with aromatic picoline ring, pi-alkyl interaction of halogen (Br) with Leu764, and strong aromatic hydrophobic interaction with Val702 residue. (Fig. 1).

In a similar fashion, the test compounds 7j (N-(1-isopropyl-7-methyl-2-oxo-4-phenyl-1,2-dihydroquinazolin-6-yl)-4-methoxybenzamide) and 7h (N-(1-isopropyl-7-methyl-2-oxo-4-phenyl-1,2-dihydroquinazolin-6-yl)thiophene-2-carboxamide) also gave reasonably good docking scores (−9.65 kcal/mol for 7j and −9.31 kcal/mol for 7h respectively) with EGFR TKD (1M17) active binding sites. The captured binding characteristics, 2D and 3D docking profiles of 7j and 7h with target protein EGFR TKD (1M17) were provided in Table 2 and Fig. 2 & Fig. 3 respectively. The docking analysis results of 7j and 7h are consistency with experimentally

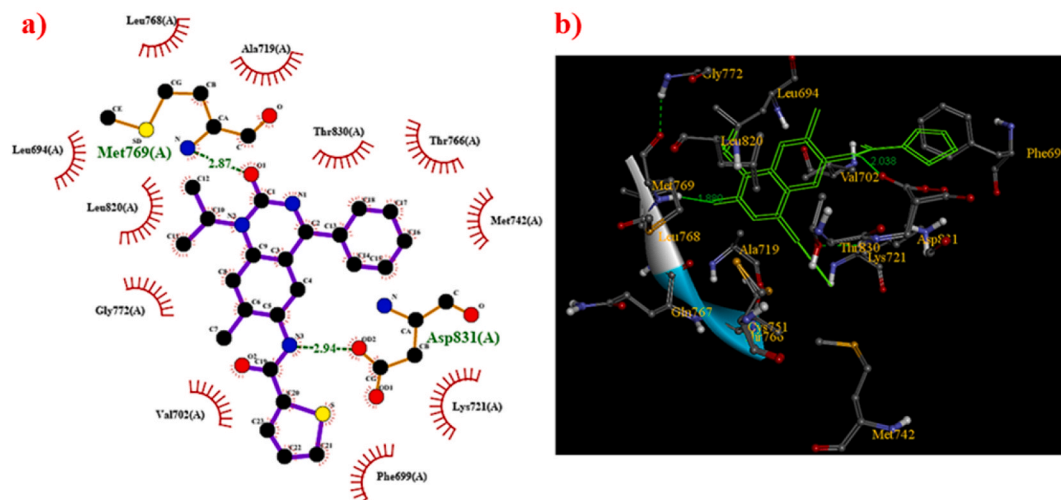


Fig. 2. 2D (left side (a)) and 3D (right side (b)) Docking interaction profiler of 7j with EGFR-TKD active site of protein(1M17).

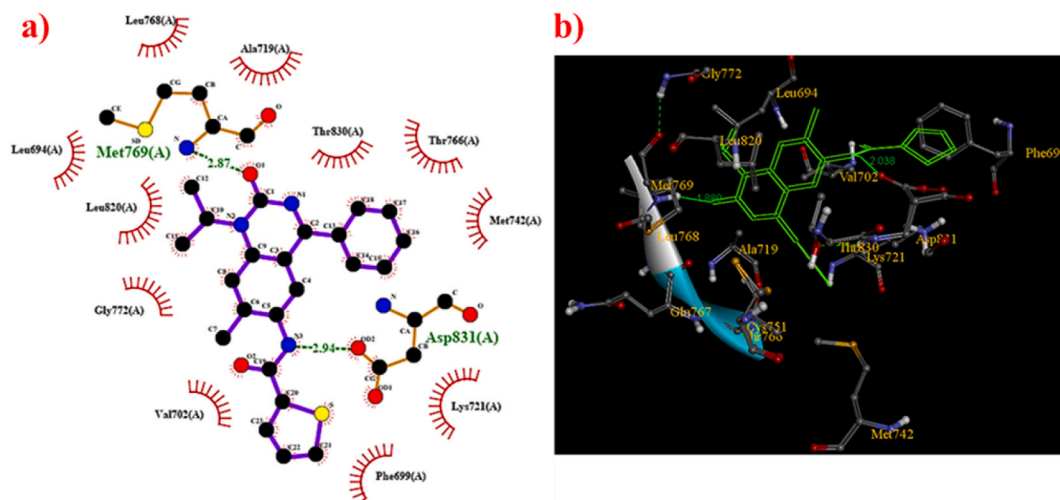


Fig. 3. 2D (left side (a)) and 3D (right side (b)) Docking interaction profiler of **7h** with EGFR-TKD active site of protein(1M17).

observed apoptotic activity on four human cancer cell lines. Both **7j** and **7h** exhibited excellent to good inhibitory activity with four human cancer cell lines tested in MTT assay compared to all other test compounds and reference standard Etoposide (See Table 1).

The molecular docking results of test compound **7g** (N-(1-isopropyl-7-methyl-2-oxo-4-phenyl-1,2-dihydroquinazolin-6-yl) thiophene-2-carboxamide) with target protein EGFR TKD (1M17) also yielded a fairly good docking score of -9.41 kcal/mol, which is quite similar to the docking score of -9.31 kcal/mol (for **7h**). Nevertheless, the compound's *in-vitro* apoptotic activity against four human cancer cell lines is found to be moderate in comparison to **7i**, **7j**, and **7h**. The molecular docking results of all other test compounds (**7a-g**) with EGFR TKD (1M17) were provided in the supplementary information. Furthermore, the test compounds (**7a-j**) were subjected to molecular docking investigation with another target protein, such as topoisomerase-II β (PDB ID: 3QX3) [59]. The resulting docking characteristics and binding interaction data were reported in Table S3 of the supplementary information.

2.4. ADME analysis

2.4.1. Pharmacokinetic properties studies (ADME)

Absorption, distribution, metabolism, and excretion (ADME) analysis predict the druggability of a molecule by studying its adherence with the 'Lipinski Five' Rules [60]. The pharmacokinetic properties and drug-likeness of novel amidic derivatives of Quinazolinone (**7a-j**) were studied and compared with standard drug (Etoposide) using an online accessible web tool: ADMET lab 2.0 and SwissADME program of the Molecular Modelling Group of the Swiss Institute of Bioinformatics [61–66] which are publicly available at <https://admet.mesh.scbdd.com> and <http://www.swissadme.ch>, respectively. The software computed various pharmacokinetic properties and descriptors: Physicochemical: Donor H-bond (nHD < 7) and acceptor H-bond (nHA < 12), n-stereo center ≤ 2 , aqueous solubility (Log S range 0.5 to -4 mol/L) and octanol/water partitioning coefficient (Log P ≤ 5); Absorption: The human colon adenocarcinoma cell lines permeability (Caco-2 > -5.15), human gastrointestinal absorption capability (HIA) range from 0 to 0.3; Distribution: Brain/blood barrier (BBB) permeability in range from 0 to 0.3 cm/s, and Topological polar surface (<140) and rule of five (Lipinski). The percentage of oral absorption (%ABS) was calculated according to the method of Zhao et al. [67]. All the derivatives (**7a-j**) have shown strong cell permeability and the highest human oral observation compared with positive control (Etoposide) (Table S4 in SI).

2.5. Molecular dynamic simulations

2.5.1. MD studies of **7h**, **7i** and **7j** drugs

The molecular mechanics studies further revealed how these quinazolinone derivatives interacted with the active site of kinase

Table 3

Mean binding energy, average binding and free energy of EGFR TKD-Quinazolinone derivative complexes of (**7h-7j**).

S. No	Quinazolinone derivative	Binding energy (kcal/mole)	MM/GBSA 100ns (kcal/mol)	Std. Err. of Mean (\pm)	MM/PBSA (kcal/mol)	Std. Err. of Mean (\pm)
1	7h	-9.31	-34.7559	0.1334	-7.5478	1.8089
2	7i	-9.67	-39.8501	0.1815	-7.6282	2.4312
3	7j	-9.65	-41.7478	0.1554	-7.4321	1.7682

domain in EGFR kinase domain. The 100 ns AMBER MD simulations trajectories of the three complexes were analyzed by root mean square deviation (RMSD) and root mean square fluctuation (RMSF) plots, and the total energy of the molecular systems. The initial and final average structures superimposed well with low RMSD in the C-terminal domain, whereas significant conformational changes were seen in the N-terminal domain of EGRF TKD (1M17). The average total energies of the complexes were nearly the same; **7h** (-9.31 kcal/mol), **7i** (-9.67 kcal/mol), and **7j** (-9.65 kcal/mol) as shown in Table 3.

The EGFR TKD-**7h** complex was the most stable complex with a low RMSD of the protein and ligand (Fig. S6 and Fig. S7) and relatively low RMSF fluctuations (Fig. S8). The N- and C- terminal regions displayed higher RMSF compared to the other regions in the protein structure. All molecules induced relatively higher distortions in EGFR protein kinase N-terminal β -sheet rich region during 100 ns MD simulations. Manual examination of the complexes from MD simulations (**7h** and **7j**) indicated that these chemical conformers moved closer towards the activation loop while the **7i** continued to bind close to the hinge region. This can be seen from the Supplementary Figs. S6–S8). As the binding affinities from free energy calculations, the **7j** has more binding affinity (-41.74 kcal/mol)

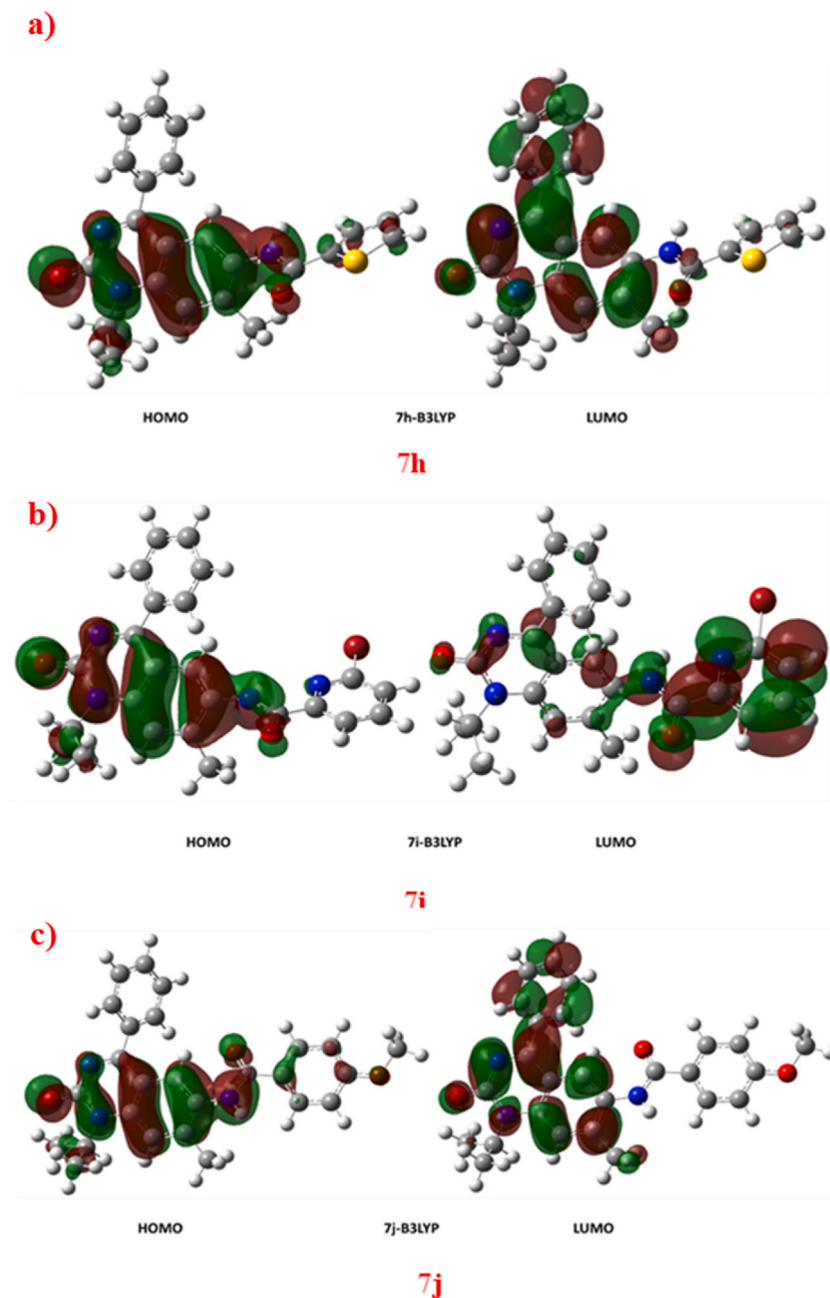


Fig 4. The frontier molecular orbital of compounds a) **7h**, b) **7i** and c) **7j** computed at B3LYP/6-31g (d,p) level in the gas phase.

Table 4

AutoDock binding energies and DFT of inhibitors and MD studies of EGFR kinase domain -inhibitor complexes.

S. No	EGFR -drug complex	ADT inhibitor mean binding energy in kcal/mol	Total Energy in DFT kcal/mole for inhibitor	The inhibitor HOMO- LUMO gap QM calculation kcal/mol	Average Total Energy of EGFR drug complex in MD 100 ns kcal/mol
01	7h	-9.31	-1.01E+06	-152.60	-91.928
02	7i	-9.67	-2.43E+06	-151.02	-91.865
03	7j	-9.65	-8.76E+05	-149.58	-91.911

among all molecules in terms of solvation surface energy from MMGBSA but in terms of polar and dispersion binding affinities, the **7i** has more PB polar and dispersion solvation binding affinity (-7.62 kcal/mol) towards the protein-inhibitor complex. The PB and GB methods calculated the binding affinities of protein-inhibitors associated with the water solvation sphere as ΔG of various terms including van der Waals, surface solvation, polar and dispersion solvation energies as given by individual differences given as $[(\Delta G \text{ Complex} - \{\Delta G \text{ Receptor} - \Delta G \text{ Ligand}\})]$ (Homeyer et al., 2012 and Wright et al., 2014) [68].

From the above analysis, **7h** and **7i** are better suitable drug candidates at hinge region inhibition whereas **7j** is bound towards the activation loop region and the highest GB binding free energy -41.74 kcal/mol showed the best drug molecule among all drug candidates. The average structure analysis of initial and final 100 ns MD simulations structures describes how the inhibitor moves towards the hinge region in **7h** and **7i** bound EGFR kinase domain. The final average structures of EGFR TKD-**7j** showed the inhibitor moved towards the kinase active binding site to influence activation and α C-helix flip movement from initial structures. Therefore, the **7j** inhibitor has shown effective binding affinity at active site of kinase domain in EGFR as high GB binding free energy. The PB energies indicated EGFR kinase domain hinge region has high polar and dispersion solvation interactions with **7i** and **7h** drug molecules rather than **7j** bound at the kinase active site region. The **7j**, **7i**, and **7h** are bound at the kinase active site region but the drug-bound effective site region may vary based upon the active chemical space environment of specified functional group attached to quinoline basic structures of given drug molecules. From the MM-GBSA analyses, the binding free energies were observed to be **7h** (-34.7559 kcal/mol), **7i** (-39.8501 kcal/mol), and **7j** (-41.7478 kcal/mol) as shown in Table 3. The in-silico results correlated reasonably well with the in vitro MTT assay observations which confirms the concurrence of data derived computational tools and experimentally derived cytotoxic in vitro results. The research findings reported by Sangpheak et al., 2019, Bandaru et al., 2021, supported that the compound **7j** (4-methoxy), with electron donating substitutions may show potent anticancer activity and derivatives having heterocyclic ring substitutions **7h** and **7i** showed potent anticancer activity.

2.6. Density functional theory

2.6.1. Quantum chemical studies of synthetic drugs

The quantum chemical optimization was done for the three synthetic inhibitors with a corrected correlation of hybrid Beckmann exchange integral from Hartree Fock-Density functional combined level theory and 6-311 + G (d, p) basis set including polarized and diffused functional of d and p-type orbitals including hydrogen atom distorted polarized functional. The highest occupied molecular orbital (HOMO) and lowest unoccupied molecular orbital (LUMO) were evaluated to understand the zone that is rich (donor) and poor (acceptor) in electrons, and the band gap energy in each of the compounds. The HOMO is observed on the quinazoline and the amide link adjacent to it. Whereas the LUMO is located on the quinazoline and connected phenyl ring in **7h** and **7j**, whereas, in **7i** the LUMO is located on the bromo-substituted pyridine ring (Fig. 4).

The HOMO-LUMO band gap energies for all three molecules vary from 152.6 to 149.58 kcal per mol (Table 4). Based on the band gap energy, we propose that **7j** has a relatively better pharmacophore entity.

3. Conclusions

A new series of amide-enriched 2-(1H)-quinazolinone derivatives (**7a-j**) were synthesized under mild reaction conditions with excellent yields. The in vitro cytotoxic potential (Apoptotic activity) of these new compounds (**7a-j**) were screened against MCF7 (breast cancer), A549 (lung cancer), PC3 (prostate cancer) and DU145 (prostate cancer). The novel amide-enriched 2-(1H)-quinazolinone derivatives **7i** and **7j** displayed good cytotoxic activities against cancer cell lines, MCF-7 and **7h** showed against PC3, with IC₅₀ values in low micromolar range. Molecular docking studies of the **7a-7j** have showed a strong binding (-9.00 to -9.67 kcal/mol) with EGFR tyrosine kinase domain with 4-anilinoquinazoline inhibitor erlotinib (1M17). Additionally, DFT investigations and MD simulations validated the predictions of molecular docking. According to the findings of the ADME analysis, oral absorption by humans is anticipated to be higher than 85 % for all test compounds. The obtained results are very promising and demonstrate that the new compounds **7i**, **7j** and **7h** could lead towards anticancer drug development.

4. Experimental section

4.1. Chemistry

General: All the reactions were carried out under an inert atmosphere with dry solvents under anhydrous conditions unless

otherwise mentioned. DCE was distilled from calcium hydride under a nitrogen atmosphere, ethanol was distilled from sodium ethoxide followed by magnesium, TEA was distilled from KOH and toluene was distilled from sodium. All the reactions were carried out under appropriate conditions and monitored by the thin layer chromatography (TLC) using silica gel on aluminum plates (GF₂₅₄) by charring with 3 % (w/v) ninhydrin in n-butanol or by 3 % (w/v) phosphomolybdic acid (PMA) stain or by ultraviolet (UV) detection. Silica-gel (100–200 mesh) was used for column chromatography to purify the compounds. ¹H spectra were recorded on Bruker® Avance 500, 400 MHz and for ¹³C 125, 100 MHz spectrometer in deuterated solvent (CDCl₃). ¹H NMR chemical shifts were reported in parts per million (ppm) (δ) with TMS as an internal standard (δ 0.00), and ¹³C NMR were reported in chemical shifts with solvent reference (CDCl₃, δ 77.00). Mass spectra were recorded on Micro mass, Quattro LC using ESI + software with capillary voltage 3.98 kV and ESI mode positive ion trap detector and High-resolution mass spectra (HRMS) were recorded on Bruker maxis ESI-TOF spectrometer. The purity of all the tested compounds (7a-j) was determined to have >95 % purity by HPLC analysis.

4.1.1. Synthesis procedure of compound 1 & 1a[2-chloro-4-methylphenyl] (phenyl)methanone & (4-chloro-2-methylphenyl) (phenyl)methanone]

To a stirred solution 0.79 mol (100 g) of compound 1 in ethylene dichloride (EDC) (2.5L) at 0–5 °C, were added 0.86 mol (100 mL) of benzoyl chloride and 0.9 mol (120g) of AlCl₃, heated the reaction mixture to 100 °C and agitated for 16 h. The progress of the reaction was monitored by TLC (E. A: Hex 4:6), Quenched the mixture with dil. HCl at 0–10 °C and extracted the compound twice with Dichloromethane (2 × 600 mL). The combined organic layer was washed with purified water and 20 % sodium chloride solution. Dried the organic layer over MgSO₄ and concentrated under reduced pressure at a temperature below 45 °C. The distilled residue was purified by flash column chromatography using (100–200 mesh silica) and gradient EtOAc/hexane to offer pure compound 1 (92.7g) and 1a (63.4g) as off-white solids with 51 % & 35 % yield respectively.

1: ¹H NMR (500 MHz, CDCl₃): δ = 7.812 (d, 2H, J = 10 Hz), 7.610 (t, 1H, J = 8.5 Hz), 7.493–7.462 (m, 2H), 7.313–7.281 (m, 2H), 7.195 (d, 1H, J = 9.8 Hz), 2.432 (s, 3H); 1a: ¹H-NMR (500 MHz, CDCl₃): δ = 7.806 (d, 2H, J = 9.5 Hz), 7.601 (t, 1H, J = 16.5 Hz), 7.471 (t, 2H, J = 14 Hz), 7.325–7.244 (m, 3H), 2.345 (s, 3H).

4.1.2. Synthesis procedure of compound 2 and 2a[2-chloro-4-methyl-5-nitrophenyl] (phenyl)methanone & 4-chloro-2-methyl-5-nitrophenyl] (phenyl)methanone]

To a stirred suspension of 0.217 mol (50g) compound 1 in 0.43 mol (42.4g) of conc. H₂ SO₄ was added 0.49 mol (50g) of acetic anhydride and cooled the mixture to –10 to –5 °C, slowly adding 0.217 mol (13.68 g) of conc. HNO₃ at –10 to –5 °C and the mixture was allowed to warm to room temperature and agitated for 3 h, the progress of the reaction was monitored by TLC (E. A: Hex 4:6). Reaction mixture was poured into crushed ice and neutralized with aq. NaOH solution.

Extracted twice with Dichloromethane (2 × 500 mL). The combined organic layer was washed with purified water, and 20 % sodium chloride solution. The organic layer was dried over MgSO₄ and concentrated under a reduced pressure temperature below 45 °C. The distilled residue was purified by flash column chromatography using (100–200 mesh silica) gradient EtOAc/hexane to offer pure compound 2 (28g) and 2a (22.7g) as pale-yellow solids with 47 % & 32.7 % yield respectively. 2: ¹H-NMR (500 MHz, CDCl₃): δ = 8.085 (s, 1H), 7.836 (d, 2H, J = 11.9 Hz), 7.694 (t, 1H, J = 20.1 Hz), 7.545–7.506 (m, 3H), 2.710 (s, 3H); 2a: ¹H-NMR (500 MHz, CDCl₃): δ = 8.595 (s, 1H), 8.591–8.512 (m, 1H), 8.184–8.140 (m, 2H), 7.743 (t, 1H, J = 16 Hz), 7.557 (s, 1H), 2.743 (s, 3H).

4.1.3. Synthesis procedure of compound 3 [2-(isopropyl amino)-4-methyl-5-nitrophenyl] (phenyl)methanone]

To a stirred solution 0.072 mol (20g) of compound 2 in Ethanol (200 mL) was added 0.18 mol (10.7g) of isopropyl amine, 0.43 mol (60g) of K₂CO₃ and 0.06 mol (12g) of CuI. The mixture was heated to 80 °C and agitated for 5h. The progress of the reaction was monitored by TLC (E. A: Hex 4:6). Diluted the mixture with purified water and extracted thrice with dichloromethane. The combined organic layer was washed with purified water, and sodium chloride solution and dried over MgSO₄. The organic layer was concentrated under reduced pressure at 40–45 °C. The distilled residue was purified by flash column chromatography using (100–200 mesh silica) gradient EtOAc/hexane to offered (15.46g) of pale-yellow solid compound 3 with 72 % yield. ¹H-NMR (500 MHz, CDCl₃): δ = 9.170 (s, 1H), 8.503 (s, 1H), 7.641–7.580 (m, 3H), 7.535–7.499 (m, 2H), 6.595 (s, 1H), 3.926–3.876 (m, 1H), 2.713 (s, 3H), 1.387–1.372 (d, 6H, J = 8.0 Hz).

4.1.4. Synthesis procedure of compound 4 [1-isopropyl-7-methyl-6-nitro-4-phenyl quinazolin-2(1H)-one]

0.033 mol (10g) of compound 3, in 50 mL of ethyl carbamate and 0.07 mol (10g) of ZnCl₂ were taken into seal tube. Heated the mixture to 240 °C and agitated for 3 h. Cooled the contents to 0–5 °C. Quenched with dil. HCl and extracted twice with Dichloromethane. Combined organic phase was dried over MgSO₄ and concentrated under reduced pressure at 40–45 °C. The distilled residue was purified by flash column chromatography using (100–200 mesh silica) gradient EtOAc/hexane to offered (7.36g) of pale-yellow solid compound 4 with 68 % yield. ¹H-NMR (500 MHz, CDCl₃): δ = 8.586 (s, 1H) 7.766–7.751 (d, 2H, J = 7.5 Hz), 7.649–7.568 (m, 3H), 7.427 (s, 1H), 5.142–5.116 (m, 1H), 2.834 (s, 3H), 1.748–1.734 (d, 6H, J = 7 Hz).

4.1.5. Synthesis procedure of compound 5 [6-amino-1-isopropyl-7-methyl-4-phenyl quinazolin-2(1H)-one]

To a solution, 0.02 mol (6.5g) of compound 4 in MeOH (100 mL) was added raney Ni (0.65g) and the mixture was hydrogenated under H₂ in at atmosphere using a bladder for 1 h. The progress of the reaction was monitored by TLC (E. A: Hex 4:6). The mixture was filtered through Celite and concentrated under a reduced pressure temperature below 45 °C. The distillate residue was purified by column chromatography using gradient EtOAc/hexane to offer (4.84g) of compound 5 as a pale yellow to beige solid with 82 % yield. ¹H-NMR (500 MHz, CDCl₃): δ = 7.719–7.70 (d, 2H, J = 9.5 Hz), 7.533–7.489 (m, 3H), 7.347 (s, 1H), 7.029 (s, 1H), 5.196 (brs, 1H),

3.655 (s, 2H), 2.380 (s, 3H), 1.711–1.697 (d, 6H, $J = 7.0$ Hz). Purity by RP- HPLC: 99.39 %, MS (ESI): Calcd. For (C₁₇ H₁₆ N₃ O) [M + H]⁺: 293.37, found 294.42.

4.2. Synthesis procedure of 7a-j

4.2.1. 2-(4-fluorophenyl)- N-(1-isopropyl-7- methyl-2-oxo-4-phenyl-1,2-di hydroquinazolin-6yl) acetamide(7a)

To a solution of (150 mg, 0.51 mmol) of compound 5 in Toluene (18 mL) was added (129.3 mg, 1.28 mmol) of TEA and (110 mg, 0.637 mmol) of 4-Fluorophenylacetyl chloride in toluene at 0–5 °C. Agitate the mixture at 0–10 °C for 30 min and slowly raise the reaction mass temperature to reflux for 2h. The mixture was neutralized with aqueous saturated sodium bicarbonate solution and the separated organic layer was washed with sodium chloride solution. Dried the organic layer over sodium sulfate and concentrated under reduced pressure at a temperature below 45 °C. The distillate residue was purified by column chromatography using gradient EtOAc/hexane to offer (149 mg) of compound 7a as off-white solid with 68 % yield. **H-NMR (500 MHz, CDCl₃)**: $\delta = 8.18$ (dd, 1H, $J = 7.2, 3.5$ Hz), 7.71 (s, 2H), 7.55–7.48 (m, 4H), 7.38–7.32 (m, 3H), 7.18–7.11 (m, 2H), 5.12 (s, 1H), 3.79 (s, 2H), 2.29 (s, 3H), 1.67 (d, 6H, $J = 7.0$ Hz); **¹³C{¹H} NMR (125 MHz, CDCl₃)**: $\delta = 173.34, 168.63, 161.92, 159.97, 155.47, 141.21, 136.16, 131.82$ – $131.79, 130.69, 129.82, 128.36, 124.84, 115.84, 48.94, 37.65, 19.14, 14.15$; **HRMS (ESI)**: (C₂₆ H₂₄ FN₃ O₂); [M + H]⁺: calcd: 430.1931, found: 430.1925. HPLC purity: 98.45 %

4.2.2. N-(1-isopropyl-7- methyl-2-oxo-4-phenyl-1,2-di hydroquinazolin-6-yl) cyclohexane carboxamide(7b)

The compound 7b was prepared by the method described for 7a, employing compound 5(150 mg, 0.51 mmol) in toluene, followed by the addition of Cyclohexane carbonyl chloride (6b) (94 mg, 0.637 mmol) to afford pure compound 7b (164 mg) as pale-yellow solid with 74 % yield. **¹H-NMR (500 MHz, CDCl₃)**: $\delta = 8.03$ (s, 1H), 7.68 (d, 2H, $J = 5.0$ Hz), 7.51–7.44 (dq, 4H, $J = 14.3, 7.1$ Hz), 7.39 (s, 1H), 5.12 (s, 1H), 2.44 (s, 3H), 2.33 (ddd, 1H, $J = 15.4, 7.8, 3.5$ Hz), 1.84–1.79 (m, 2H), 1.67 (d, 6H, $J = 7.5$ Hz), 1.56–1.49 (m, 2H), 1.28 (d, 6H, $J = 15.5$ Hz); **¹³C{¹H} - NMR (125 MHz, CDCl₃)**: $\delta = 175.12, 173.28, 165.53, 155.51, 141.23, 136.18, 130.65$ – $129.79, 128.37, 125.43, 115.73$ – $115.28, 48.97, 45.87, 29.73, 25.66, 19.38, 14.14$; **HRMS (ESI)**: (C₂₅ H₂₉ N₃ O₂); [M + H]⁺: calcd: 434.2338, found: 434.2334. HPLC purity: 99.01 %.

4.2.3. N-(1-isopropyl-7-methyl-2-oxo-4-phenyl-1, 2-di hydroquinazolin-6-yl) benzamide (7c)

The compound 7c was prepared by the method described for 7a, employing compound 5(150 mg, 0.51 mmol) in toluene, followed by the addition of benzoyl chloride (6c) (89.6 mg, 0.637 mmol) to afford pure compound 7c (142 mg) as pale-yellow solid with 70 % yield. **¹H-NMR (400 MHz,**

CDCl₃): $\delta = 8.73$ (s, 1H), 7.98 (d, 3H, $J = 4.2$ Hz), 7.62 (d, 2H, $J = 8.4$ Hz), 7.54–7.39 (m, 6H), 5.07 (s, 1H), 2.53 (s, 3H), 1.64 (d, 6H, $J = 6.0$ Hz); **¹³C{¹H} - NMR (100 MHz, CDCl₃)**: $\delta = 173.15, 166.59, 155.58, 141.54, 135.99, 134.12, 130.70, 129.78, 128.68, 127.56, 126.13, 127.3, 126.13$ – 115.84 – $115.25, 49.11, 19.68$; **HRMS (ESI)**: (C₂₅ H₂₃ N₃ O₂); [M + H]⁺: calcd: 398.1868, found: 398.1862. HPLC purity: 98.74 %.

4.2.4. 3-Bromo-N-(1-isopropyl-7-methyl-2-oxo-4-phenyl-1,2-di hydroquinazolin-6yl) benzamide (7d)

The compound 7d was prepared by the method described for 7a, employing compound 5(150 mg, 0.51 mmol) in toluene, followed by addition of 3-bromobenzoyl chloride (6d) (140 mg, 0.637 mmol) to afford pure compound 7d (189 mg) as beige solid with 78 % yield. **¹H-NMR (500 MHz, CDCl₃)**: $\delta = 8.63$ (s, 1H), 8.10 (s, 1H), 7.93 (s, 1H), 7.89 (d, 1H, $J = 7.8$ Hz), 7.64 (ddd, 1H, $J = 7.9, 2.0, 1.0$ Hz), 7.57 (d, 2H, $J = 7.5$ Hz), 7.44–7.35 (m, 4H), 7.31 (t, 1H, $J = 7.9$ Hz), 5.06 (s, 1H),

2.51 (s, 3H), 1.63 (d, 6H, $J = 6.9$ Hz); **¹³C{¹H} - NMR (100 MHz, CDCl₃)**: $\delta = 173.13, 165.12, 155.58, 141.63, 136.05, 135.90, 134.96, 130.76, 130.33, 129.72, 128.36, 126.24, 115.92$ – $115.26, 49.18, 19.67, 14.52$; **HRMS (ESI)**: (C₂₅ H₂₂ Br N₃ O₂); [M + H]⁺: calcd: 476.0973, found: 476.0969. HPLC purity: 98.26 %.

4.2.5. 3,2,5 N-(1-isopropyl-7- methyl-2-oxo-4-phenyl-1,2-di hydroquinazolin-6-yl)-4methyl benzamide (7e)

The compound 7e was prepared by the method described for 7a, employing compound 5(150 mg, 0.51 mmol) in toluene, followed by addition of 4- methylbenzoyl chloride (6e) (99 mg, 0.637 mmol) to afford pure compound 7e (145 mg) as pale-yellow solid with 69 % yield. **¹H-NMR (500 MHz, CDCl₃)**: $\delta = 8.20$ (s, 1H), 7.78 (d, 5H, $J = 8.4$ Hz), 7.58–7.48 (m, 3H), 7.45 (s, 1H), 7.29 (d, 2H, $J = 8.0$ Hz), 5.16 (s, 1H), 2.52 (s, 3H), 2.43 (s, 3H), 1.70 (d, 6H, $J = 7.2$ Hz); **¹³C{¹H} - NMR (125 MHz, CDCl₃)**: $\delta = 173.13, 166.36, 155.54, 142.03, 136.08, 131.22, 130.68, 129.81, 129.40, 127.41, 125.86, 115.54, 49.03, 21.53, 19.56$; **HRMS (ESI)**: (C₂₆ H₂₅N₃ O₂); [M + H]⁺: calcd:

412.2025, found: 412.2020. HPLC purity: 98.97 %.

4.2.6. 2-(4-bromophenyl)- N-(1-isopropyl-7- methyl-2-oxo-4-phenyl-1,2-di hydroquinazolin-6yl) acetamide (7f)

The compound 7f was prepared by the method described for 7a, employing compound 5(150 mg, 0.51 mmol) in toluene, followed by the addition of 4- bromophenylacetyl chloride (6f) (149 mg, 0.637 mmol) to afford pure compound 7f (180 mg) as light brown solid with 72 % yield. **¹H- NMR (500 MHz, CDCl₃)**: $\delta = 8.16$ (s, 1H), 7.75–7.71 (m, 2H), 7.55–7.50 (m, 5H), 7.34 (s, 1H), 7.23 (d, 2H, $J = 8.4$ Hz), 7.08 (s, 1H), 5.11 (s, 1H), 3.72 (s, 2H), 2.20 (s, 3H).1.67 (d, 6H, $J = 7.0$ Hz); **¹³C{¹H} -NMR (125 MHz, CDCl₃)**: $\delta = 173.39, 169.61, 155.29, 141.21, 140.57, 135.94, 133.90, 130.28$ – 132.23 (m), 129.67, 128.33, 125.35, 121.35, 115.44, 49.12, 43.19, 19.35, 15.26; **HRMS (ESI)**: (C₂₆ H₂₄ Br N₃ O₂); [M + H]⁺: calcd: 490.1130, found: 490.1141. HPLC purity: 98.58 %.

4.2.7. 2-(4-bromophenyl)-N-(1-isopropyl-7-methyl-2-oxo-4-phenyl-1,2-dihydroquinazolin-6-yl)acetamide (7g)

The compound **7g** was prepared by the method described for **7a**, employing compound **5** (150 mg, 0.51 mmol) in toluene, followed by addition of Phenylacetyl chloride (**6g**) (99 mg, 0.637 mmol) to afford pure compound **7g** (160 mg) as pale-yellow solid with 76 % yield. ¹H-NMR (500 MHz, CDCl₃): δ = 8.28 (s, 1H), 7.78–7.74 (m, 2H), 7.56–7.50 (m, 3H), 7.47–7.40 (m, 2H), 7.40–7.31 (m, 4H), 6.98 (s, 1H), 5.12 (s, 1H), 3.77 (s, 2H), 2.10 (s, 3H), 1.66 (d, 6H, *J* = 7.0 Hz); ¹³C{¹H}-NMR (125 MHz, CDCl₃): δ = 173.36, 169.65, 155.45, 141.09, 138.33, 136.24, 134.48, 130.73, 129.87, 129.63, 129.41, 128.39, 115.50, 48.91, 44.48, 19.37, 18.75; HRMS (ESI): (C₂₆H₂₅N₃O₂); [M + H]⁺: calcd: 412.2025, found: 412.2026. HPLC purity: 98.73 %.

4.2.8. N-(1-isopropyl-7-methyl-2-oxo-4-phenyl-1,2-dihydroquinazolin-6-yl)thiophene-2-carboxamide (7h)

The compound **7h** was prepared by the method described for **7a**, employing compound **5** (150 mg, 0.51 mmol) in toluene, followed by addition of thiophene-2-carbonyl chloride (**6h**) (94 mg, 0.637 mmol) to afford pure compound **7h** (123 mg) as pale-yellow solid with 60 % yield. ¹H-NMR (500 MHz, CDCl₃): δ = 8.10–7.91 (m, 2H), 7.71 (dt, 3H, *J* = 16.3, 6.6 Hz), 7.56 (dt, *J* = 3.8, 1.9 Hz, 1H), 7.51–7.40 (m, 4H), 7.13 (dd, 1H, *J* = 5.1, 3.6 Hz), 5.11 (s, 1H), 2.53 (s, 3H), 1.67 (d, 6H, *J* = 6.8 Hz); ¹³C{¹H}-NMR (125 MHz, CDCl₃): δ = 173.16, 160.60, 155.53, 141.07, 138.42, 136.05, 130.78, 129.89, 129.20, 128.44, 127.99, 125.71, 115.91, 115.34, 49.10, 19.51; HRMS (ESI): (C₂₃H₂₁N₃O₂S); [M+H]⁺: calcd: 404.1432, found: 412.1422. HPLC purity: 98.09 %.

4.2.9. 3-bromo-N-(1-isopropyl-7-methyl-2-oxo-4-phenyl-1,2-dihydroquinazolin-6-yl)benzamide (7i)

The compound **7i** was prepared by the method described for **7a**, employing compound **5** (150 mg, 0.51 mmol) in toluene, followed by the addition of 6-bromopicolinoyl chloride (**6i**) (129 mg, 0.637 mmol) to afford pure compound **7i** (151 mg) as brown solid with 62 % yield. ¹H-NMR (500 MHz, CDCl₃): δ = 9.74 (s, 1H), 8.58 (s, 1H), 8.21 (d, 1H, *J* = 7.5 Hz), 7.92–7.75 (m, 3H), 7.69 (d, 1H, *J* = 7.8 Hz), 7.61–7.43 (m, 4H), 5.19 (s, 1H), 2.59 (s, 3H), 1.73 (d, 6H, *J* = 6.9 Hz); ¹³C{¹H}-NMR (125 MHz, CDCl₃): δ = 173.38, 160.78, 155.37, 150.53, 141.16, 140.54, 140.09, 138.02, 136.37, 131.30, 130.70, 129.89, 129.76, 128.40, 123.06, 121.52, 130.76, 130.33, 130.25, 129.72, 128.36, 126.24, 115.91, 48.94, 19.45; HRMS (ESI): (C₂₄H₂₁BrN₄O₂); [M + H]⁺: calcd: 477.0926, found: 477.0924. HPLC purity: 98.69 %.

4.2.10. N-(1-isopropyl-7-methyl-2-oxo-4-phenyl-1,2-dihydroquinazolin-6-yl)-4-methoxybenzamide (7j)

The compound **7j** was prepared by the method described for **7a**, employing compound **5** (150 mg, 0.51 mmol) in toluene, followed by addition of 4-methoxybenzyl chloride (**6j**) (109 mg, 0.637 mmol) to afford pure compound **7j** (179 mg) as pale-yellow solid with 82 % yield. ¹H-NMR: (400 MHz, CDCl₃): δ = 8.10 (d, 1H, *J* = 19.2 Hz), 7.94 (d, 2H, *J* = 7.3 Hz), 7.75 (d, 2H, *J* = 7.1 Hz), 7.58–7.41 (m, 4H), 7.30 (d, 1H, *J* = 3.5 Hz), 6.93–7.07 (m, 2H), 5.14 (s, 1H), 3.90 (s, 3H), 2.55 (s, 3H), 1.71 (d, 6H, *J* = 6.8 Hz); ¹³C{¹H}-NMR (100 MHz, CDCl₃): δ = 173.21, 162.73, 155.53, 141.42, 136.15, 130.63, 129.86, 129.23, 128.42, 126.25, 125.51, 115.64, 114.03, 55.53, 49.04, 19.55, 14.26; HRMS (ESI): (C₂₆H₂₅N₃O₃); [M + H]⁺: calcd: 428.1974, found: 428.1969. HPLC purity: 98.53 %.

4.3. MTT assay

The cells were plated in 96-well plates at a density of 2.0×10^4 in 200 μL of medium per well of 96 well plate. Cultures were incubated with different concentrations of test material and incubated for 48h. After the removal of old medium, 100 μL fresh medium provided for our test compound derivatives and standard drug at various concentrations like 0.05 μM, 0.1 μM, 0.5 μM, 1 μM, and 2 μM respectively. Now it was added to each well and allowed for incubation at 37 °C over 24 h time period. Now the medium was removed and restore with 10 μL MTT dye. Again, the platers were allowed for incubation at 37 °C over 2h time period. The outcoming formazan crystals were dissolved in 100 μL extracted buffer. Optical density (O.D) was recorded at 570 nm with Multi-mode Varioskan Instrument-Thermo Scientific micro plate reader. In medium, % of DMSO not exceeded to 0.25 %.

4.4. Molecular docking studies

AutoDock 4.2.6 uses the Lamarckian Genetic Algorithm (LGA) as a search engine to automate docking investigations. The pdbqt files for the receptor and the ligand were prepared using the graphical interface of the auto-docking application ADT4. 2. The 2D structures (**7a-j**) of the target compounds were generated in ChemDraw and saved as pdb files. The ligand files were subjected to energy minimization (force field-uff) using the open babel tool and conformers (autodock pdbqt files) were then generated in auto dock tool. From the protein data bank (rcsb.com/pdb database), the x-ray crystal structure of EGFR TKD in association with co-crystal "Erlotinib" [55,56] was obtained (1M17). The co-crystal (Erlotinib) and the molecular waters were eliminated. The Ramachandran plot generated using Discovery Studio was used to examine the protein for any structural issues and to check for any missing amino acids residues. All hydrogens were added, non-polar hydrogens were merged, Kollman charges were added, and missing atoms were added and assigned the AD4 type. The three-dimensional energy scoring grids with a resolution of 0.375 Å and dimensions of 60 Å - 60 Å - 60 Å were computed, and the xyz coordinates of co-crystal (Erlotinib) were extracted from Discovery studio (X = 20.676, Y = 9.289, and Z = 55.459) to generate a grid box around the region where the co-crystal ligand exhibits interactions with amino acid residues in target. Docking was done using the LGA default settings.

4.5. Molecular dynamics simulations

All MD simulations were carried out with AMBER 18.14 version packages [69]. The best docking pose of each protein-inhibitor

complex was utilized as input for MD simulations. The AMBER14SB force fields were generated for the entire system with Ante-chamber using am1bcc method [70]. All input parameter files for MD simulations were generated after adding hydrogen atoms in tLEaP module in AMBER tools at pH 7.4 [71]. Chloride ions were added to the systems to neutralize the charge, each molecular system was solvated allowing 8 Å marginal distance between the protein and side of cubic box. The overall prmtop files were verified with parmed and cpptraj to avoid any structural errors in the protein-inhibitor complex buried in the water sphere. The final ionic concentration for the systems was set to 100 mM. The Amberff14sb-ILDN force field was used for the entire model system with TIP3P water model for AMBER molecular parameters [72]. All MD simulations were run at 300 K temperature and 1 atm pressure with Monte Carlo barostat [73]. Energy minimization was carried out by using the steepest descent method for 80 000 cycles to overcome short-range null contacts among the molecular system in the solvent [74]. Long-range electrostatic interactions were considered with the Particle Mesh Ewald algorithm [75] with a cut-off range 9 Å and order 4. All model systems were equilibrated for 7 ns before the production run, and the coordinates in the production run were saved every 10ps [76]. The MD simulations of each molecular system were carried out for 100 ns, accounting for a total of 300 ns of simulation time.

The Molecular Mechanics–Generalized Born Surface Area (MM-GBSA) and Molecular Mechanics Poisson–Boltzmann Surface Area (MM-PBSA) calculations are carried out on 2k conformers from 10k frames of 100 ns MD simulations data in AMBER MMPBSA. py module. It is an efficient and user-accessible end-state free energy calculation algorithm which are inbuilt in AMBER18 tools. The end-state implicit solvents model free energy calculations are further divided into three categories Generalized- Born (GB) and Poisson-Boltzmann (PB), Reference Interaction Site Model (RI-SM). The overall end-state single ensemble free energies calculation is a representation of each frame extracted from MD simulations data. In the current work, free energy calculations have been done with single trajectory protocol (STP) where 2k frames of comparable ensembles were taken from individual 100 ns MD simulations data of the bound and unbound states between receptor and inhibitor complexes [77].

4.6. Quantum chemical calculations

The molecular structures of **7h-7j** were sketched using ChemDraw 22.0 and hydrogen atoms were added. The 3D structures were quantum optimized using G09 quantum mechanical suite with hybrid DFT level of theory [CAM- B3LYP], basis set 6-311 + G*(d, p) overall complex charge zero and spin multiplicity assigned for G09 quantum mechanical calculations [78,79]. Molecular orbital analysis was performed at the B3LYP/6-311 + G(2d, p) level of theory, to evaluate the HOMO and LUMO for all the molecules obtained through MD simulations. The ground state optimized structures including fchk files were analyzed to generate the HOMO- LUMO and their total energies. This analysis was carried out to identify the zone that is electron-rich in the considered molecules.

4.7. ADME analysis

Absorption, distribution, metabolism, and excretion (ADME) analysis predict the druggability of a molecule by studying its adherence with the 'Lipinski Five' Rules [60]. The pharmacokinetic properties and drug-likeness of novel amidic derivatives of Quinazolinone (7a-j) were studied and compared with standard drug (Etoposide) using an online accessible web tool: ADMET lab 2.0 and SwissADME program of the Molecular Modelling Group of the Swiss Institute of Bioinformatics [61–66] which are publicly available at <https://admet.mesh.scbdd.com> and <http://www.swissadme.ch>, respectively. The software computed various pharmacokinetic properties and descriptors: Physicochemical: Donor H-bond (nHD <7) and acceptor H-bond (nHA <12), n-stereo center ≤2, aqueous solubility (Log S range 0.5 to –4 mol/L) and octanol/water partitioning coefficient (Log P ≤ 5); Absorption: The human colon adenocarcinoma cell lines permeability (Caco-2 > –5.15), human gastrointestinal absorption capability (HIA) range from 0 to 0.3; Distribution: Brain/blood barrier (BBB) permeability in range from 0 to 0.3 cm/s, and Topological polar surface (<140) and rule of five (Lipinski).

Funding statement

This research did not receive any specific grant from funding agencies in the public, commercial, or not-for-profit sectors.

Data availability statement

Data included in article/supplementary material/referenced in article.

CRediT authorship contribution statement

Naganjaneyulu Gariganti: Visualization, Validation, Methodology, Investigation, Formal analysis, Data curation, Conceptualization. **Anjaneyulu Bandi:** Formal analysis, Data curation. **K.R.S. Naresh Gatta:** Software, Formal analysis, Data curation. **Jishu Pagag:** Software, Formal analysis, Data curation. **Lalitha Guruprasad:** Writing – review & editing, Supervision, Software, Formal analysis, Data curation. **Bhaskar Poola:** Writing – review & editing, Validation, Supervision, Project administration, Conceptualization. **Ravi K. Kottalanka:** Writing – review & editing, Writing – original draft, Project administration, Funding acquisition, Data curation, Conceptualization.

Declaration of competing interest

The authors declare that they have no known competing financial interests or personal relationships that could have appeared to influence the work reported in this paper.

Acknowledgements

The authors would like to thank the Advanced Research Center-AMMPC, Department of Chemistry, VFSTR, Neuland Laboratories Ltd. and University of Hyderabad for providing instrumentation, research and CMSD for computational facilities. Special thanks to Shiva K. Loke, J. Anjaneyulu and Rajiv Kamaraj for their essential recommendations for creating graphical abstract.

Appendix A. Supplementary data

Supplementary data to this article can be found online at <https://doi.org/10.1016/j.heliyon.2024.e30292>.

References

- [1] C.P. Wild, E. Weider pass, B.W. Stewart, World Cancer Report: Cancer Research for Cancer Prevention" World Cancer Reports (2020). <https://shop.iarc.fr/products/world-cancer-report-cancer-research-for-cancer-prevention-pdf>.
- [2] H. Sung, J. Ferlay, R.L. Siegel, M. Laversanne, I. Soerjomataram, A. Jemal, F. Bray, Global cancer statistics. GLOBOCAN estimates of incidence and mortality worldwide for 36 cancers in 185 countries, *Ca - Cancer J. Clin.* 71 (3) (2021) 209–249, <https://doi.org/10.3322/caac.21660>.
- [3] R.L. Siegel, K.D. Miller, H.E. Fuchs, A. Jemal, Cancer statistics, *Ca - Cancer J. Clin.* 71 (1) (2021) 7–33, <https://doi.org/10.3322/caac.21708>.
- [4] T.T. Tok, S.K. Gowder, Anticancer drug—friend or foe, *Pharmacol. Therapeut.* Chapter 9 (2014) 256–269, <https://doi.org/10.5772/58552>.
- [5] G. M. Cooper, E. Robert, Hausman, A molecular approach. The Cell. second ed. Sunderland, MA: Sinauer Associates. <https://www.ncbi.nlm.nih.gov/books/NBK9839/>.
- [6] I. Ahmad Shagufta, Recent insight into the biological activities of synthetic xanthone derivatives, *Eur. J. Med. Chem.* 116 (2016) 267–280, <https://doi.org/10.1016/j.ejmech.2016.03.058>.
- [7] I. Ahmad, Shagufta, recent developments in steroidal and nonsteroidal aromatase inhibitors for the chemoprevention of estrogen-dependent breast cancer, *Eur. J. Med. Chem.* 102 (2015) 375–386, <https://doi.org/10.1016/j.ejmech.2015.08.010>.
- [8] I. Ahmad, Shagufta, an important class of organic compounds with diverse biological activities, *Int. J. Pharm. Sci.* 7 (2015) 19–27. <https://journals.innovareacademics.in/index.php/ijpps/article/view/4603/8498>.
- [9] R. Oliver, Heterocyclic chemistry – a mature Area in its infancy, *Eur. J. Org. Chem.* 3132 (2019) 4973–4975, <https://doi.org/10.1002/ejoc.201901162>.
- [10] A.M. Jawaid, Y.M. Shahar, K.A. Ahmed, Z. Ali, M.R. Haider, Recent advances in the synthesis and anticancer activity of some molecules other than nitrogen containing heterocyclic moieties, *Mini Rev Med Chem* 17 (17) (2017) 1602–1632, <https://doi.org/10.2174/1389557516666161031121639>.
- [11] J. Jampilek, Heterocycles in medicinal chemistry, *Molecules* 24 (21) (2019) 3839, <https://doi.org/10.3390/molecules24213839>.
- [12] R.R. Varma, J.G. Pandya, F.U. Vaidya, C. Pathak, B.S. Bhatt, M.N. Patel, Biological activities of pyrazoline-indole based Re(I) carbonyls: DNA interaction, antibacterial, anticancer, ROS production, lipid peroxidation, in vivo and in vitro cytotoxicity studies, *Chem. Biol. Interact.* 330 (2020) 109231, <https://doi.org/10.1016/j.cbi.2020.109231>.
- [13] P. Jia, R. Ouyang, P. Cao, X. Tong, X. Zhou, T. Lei, S. Zhou, Recent advances and future development of metal complexes as anticancer agents, *J. Coord. Chem.* 70 (13) (2017) 2175–2201, <https://doi.org/10.1080/00958972.2017.1349313>.
- [14] P. Martins, J. Jesus, S. Santos, L.R. Raposo, C. Roma- Rodrigues, P.V. Baptista, A.R. Fernandes, Heterocyclic anticancer compounds: recent advances and the paradigm shift towards the use of nanomedicine's tool box, *Molecules* 20 (9) (2015) 16852–16891, [10.3390/molecules200916852](https://doi.org/10.3390/molecules200916852).
- [15] G. Naganjaneyulu, S.K. Loke, P. Eswar, C. Poojitha, P. Bhaskar, C. Prabhakar, A. Bansal, B. Ramachandran, V. Srinivasadesikan, R.K. Kottalanka, Design, synthesis, anticancer activity of new amide derivatives derived from 1, 2, 3-triazole-benzofuran hybrids: an insight from molecular docking, molecular dynamics simulation and DFT studies, *J. Mol. Structure.* 1273 (2023) 134250.
- [16] S. Zare, L. Emami, Z. Faghih, F. Zargari, Z. Faghih, S. Khabnadideh, Design, synthesis, computational study and cytotoxic evaluation of some new quinazoline derivatives containing pyrimidine moiety, *Sci. Rep.* 13 (1) (2023) 14461, <https://doi.org/10.1038/s41598-023-41530-6>.
- [17] A. Dutta, D. Sarma, Recent advances in the synthesis of Quinazoline analogues as Anti-TB agents, *Tuberculosis* 124 (2020) 101986, <https://doi.org/10.1016/j.tube.2020.101986>.
- [18] L. Emami, S. Khabnadideh, Z. Faghih, F. Farahvasi, F. Zonobi, S.Z. Gheshlaghi, S. Daili, A. Ebrahimi, Z. Faghih, Synthesis, biological evaluation, and computational studies of some novel quinazoline derivatives as anticancer agents, *B.M.C. Chem.* 16 (1) (2022) 100, <https://doi.org/10.1186/s13065-022-00893-z>.
- [19] C. Mohan, J. Robinson, S. Kumari, Babita, R. Saxena, J. Batra, The medicinal functionality of quinazolines, *J. Pharm. Negat. Results* (2022) 1736–1742, <https://doi.org/10.47750/pnr.2022.13.S06.228>.
- [20] Y. Bansal, N. Kaur, G. Bansal, Six-membered ring (with N, O or S) fused pyrimidine-based derivatives and biological properties, *Fused Pyrimidine- Based Drug Discovery* (2023) 193–220, <https://doi.org/10.1016/B978-0-443-18616-5.00012-0>.
- [21] A. Hameed, M. Al-Rashida, M. Uroos, S.A. Ali, Arshia, M. Ishtiaq, K.M. Khan, Quinazoline and quinazolinone as important medicinal scaffolds: a comparative patent review (2011–2016), *Expert Opin. Ther. Pat.* 4 (2018) 281–297, <https://doi.org/10.1080/13543776.2018.1432596>.
- [22] F. Taayoshi, A. Iraj, A. Moazzam, M. Soleimani, M. Asadi, K. Pedrood, M. Akbari, H. Salehabadi, B. Larjani, N. Adib pour, M. Mahdavi, Synthesis, molecular docking, and cytotoxicity of quinazolinone and dihydroquinazolinone derivatives as cytotoxic agents, *B.M.C. Chem.* 16 (1) (2022) 35, <https://doi.org/10.1186/s13065-022-00825-x>.
- [23] M.A. El-Atawy, N.A. Alshaye, N. Elrubi, E.A. Hamed, A.Z. Omar, Pyrimidines-based heterocyclic compounds: synthesis, cytotoxicity evaluation and molecular docking, *Molecules* 27 (15) (2022) 4912.
- [24] H.A. Abuelizz, M. Marzouk, H. Ghabbour, R.A. Salahi, Synthesis and anticancer activity of new quinazoline derivatives, *Saudi Pharmaceut. J.* 25 (7) (2017) 1047–1054, <https://doi.org/10.1016/j.jsps.2017.04.022>.
- [25] C.R.M. Asquith, N. Fleck, C.D. Torrice, D.J. Crona, C. Grundner, W.J. Zuercher, Anti-tubercular activity of novel 4-anilinoquinolines and 4-anilinoquinazolines, *Bioorg. Med. Chem. Lett.* 29 (18) (2019) 2695–2699, <https://doi.org/10.1016/j.bmcl.2019.07.012>.
- [26] R. Komarla, N.D. Nizamuddin, A. Surur, Y.T. Mekonnen, Synthesis, characterization, antitubercular and antibacterial activity, and molecular docking of 2, 3-disubstituted quinazolinone derivatives, *Res. Rep. Med. Chem.* (2016) 15–26, <https://doi.org/10.2147/RRMC.S91474>.
- [27] A. Dutta, P. Trivedi, P.S. Gehlot, D. Gogoi, R. Hazarika, P. Chetia, D. Sarma, Design and synthesis of quinazolinone-triazole hybrids as potent anti-tubercular agents, *ACS Appl. Bio Mater.* 5 (9) (2022) 4413–4424, <https://doi.org/10.1021/acsbm.2c00562>.

- [28] B. Laleu, Y. Akao, A. Ochida, S. Duffy, L. Lucantoni, D.M. Shackelford, M. Kamaura, Discovery and structure–activity relationships of quinazolinone-2-carboxamide derivatives as novel orally efficacious antimalarials, *J. Med. Chem.* 64 (17) (2021) 12582–12602.
- [29] N. Krishnarth, S.K. Verma, A. Chaudhary, Synthesis and anti-inflammatory activity of some novel quinazolinone derivatives, *Fab J. Pharm. Sci.* 45 (3) (2020) 205–210, <https://dergi.fabad.org.tr/pdf/volum45/Issue3/205-210.pdf>.
- [30] A.A.-M. Abdel-Aziz, L.A. Abou-Zeid, K.E.H. ElTahir, M.A. Mohamed, M.A. Abu El-Enin, A.S. El-Azab, Design, synthesis of 2, 3-disubstituted 4 (3H)-quinazolinone derivatives as anti-inflammatory and analgesic agents: COX-1/2 inhibitory activities and molecular docking studies, *Bioorg. Med. Chem.* 24 (16) (2016) 3818–3828, <https://doi.org/10.1016/j.bmc.2016.06.026>.
- [31] G. Srikanth, T.V. Lakshmi, S. Nanduri, 4 (3H)-Quinazolinone derivatives: promising antibacterial drug leads, *Eur. J. Med. Chem.* 170 (2019) 157–172, <https://doi.org/10.1016/j.ejmech.2019.03.018>.
- [32] N.A. Noureldin, H. Kothayer, E.S.M. Lashine, M.M. Baraka, W.E. Eraky, S.A.E. Awdan, Synthesis, anticonvulsant activity, and SAR study of novel 4-quinazolinone derivatives, *Arch. Pharm. (Weinheim)* 350 (2) (2017) 1600332, <https://doi.org/10.1002/ardp.201600332>.
- [33] S. Pathak, V. Malhotra, R. Nath, K. Shanker, Synthesis and antihypertensive activity of novel quinazolin-4(3H)-one derivatives, *Cent. Nerv. Syst. Agents Med. Chem.* 14 (1) (2014) 34–38, <https://doi.org/10.2174/1871524914666140825144729>.
- [34] M.U. Rahman, A. Rathore, A.A. Siddiqui, G. Parveen, M.S. Yar, Synthesis and characterization of quinazolinone derivatives: search for hybrid molecule as diuretic and antihypertensive agents, *J. Enzym. Inhib. Med. Chem.* 29 (5) (2014) 733–743, <https://doi.org/10.3109/14756366.2013.845820>.
- [35] A. Ibrahim, H.M. Sakr, R.R. Ayyad, M.M. Khalifa, Design, synthesis, in-vivo anti-diabetic activity, in-vitro α -glucosidase inhibitory activity and molecular docking studies of some quinazolinone derivatives, *ChemistrySelect* 7 (14) (2022) e202104590, <https://doi.org/10.1016/j.molstruc.2021.131768>.
- [36] M. Safakish, Z. Haji Mahdi, M.R. Agha Sadeghi, R. Vahabpour, A. Zarghi, Design, synthesis, molecular modeling and anti-HIV assay of novel quinazolinone incorporated coumarin derivatives, *Curr. HIV Res.* 18 (1) (2020) 41–51, <https://doi.org/10.3109/14756366.2012.755622>.
- [37] W. Li, X. Sun, Recent advances in developing novel anti-cancer drugs targeting tumor hypoxic and acidic microenvironments, *Recent Pat. Anti-Cancer Drug Discov.* 13 (4) (2018) 455–468, <https://doi.org/10.2174/1574892813666180831102519>.
- [38] S.K. Ramadan, E.Z. Elrazaz, K.A. Abouzid, A.M.E. Naggar, Design, synthesis and in silico studies of new quinazolinone derivatives as antitumor PARP-1 inhibitors, *RSC advances* 10 (49) (2020) 29475–29492, <https://doi.org/10.1039/D0RA05943A>.
- [39] A. Sonousi, R.A. Hassan, E.O. Osman, A.M. Abdou, S.H. Emam, Design and synthesis of novel quinazolinone-based derivatives as EGFR inhibitors with antitumor activity, *J. Enzym. Inhib. Med. Chem.* 37 (1) (2022) 2644–2659, <https://doi.org/10.1080/14756366.2022.2118735>.
- [40] J. Mravljak, L. Slavec, M. Hrast, M. Sova, Synthesis and evaluation of antioxidant properties of 2-substituted quinazolin-4(3H)-ones, *Molecules* 26 (21) (2021) 6585, [10.3390%2Fmolecules26216585](https://doi.org/10.3390%2Fmolecules26216585).
- [41] N.N. Mochulskaya, E.V. Nosova, V.N. Charushin, Antiviral agents–benzazine derivatives, *Chem Heterocycl Compd (N Y)* 57 (4) (2021) 374–382, [10.1007/2Fs10593-021-02915-5](https://doi.org/10.1007/2Fs10593-021-02915-5).
- [42] P. Bhatia, V. Sharma, O. Alam, A. Manaitiyya, P. Alam, M.T. Alam, M. Imran, Novel quinazolinone-based EGFR kinase inhibitors: a review focusing on SAR and molecular docking studies (2015–2019), *Eur. J. Med. Chem.* 204 (2020) 112640.
- [43] V. Alagarsamy, K. Chitra, G. Saravanan, V. Raja Solomon, M.T. Sulthana, B. Narendhar, An overview of quinazolines: Pharmacological significance and recent developments 151 (2018) 628–685, <https://doi.org/10.1016/j.ejmech.2018.03.076>.
- [44] M. Seifaddini, P.R. Farghadani, F. Namvar, J.B. Mohamad, N.A. Muhamad, In vitro and in vivo anticancer activity of the most cytotoxic fraction of pistachio hull extract in breast cancer, *Molecules* 25 (8) (2020) 1776, <https://doi.org/10.3390/molecules25081776>.
- [45] D.H. Gandhi, F.U. Vaidya, C. Pathak, T.N. Patel, B.S. Bhatt, Mechanistic insight of cell anti-proliferative activity of fluoroquinolone drug-based Cu(II) complexes, *Mol. Divers.* 26 (2022) 869–878, <https://doi.org/10.1007/s11030-021-10199-2>.
- [46] H. Wu, L.S. Wang, P. Li, J. Yu, S. Cheng, G. Yu, B.X. Xu, Discovery of novel N-aryl-2-trifluoromethyl-quinazolinone-4-amine derivatives as the inhibitors of tubulin polymerization in leukemia cells, *Eur. J. Med. Chem.* 256 (2023) 115470, <https://doi.org/10.1016/j.ejmech.2023.115470>.
- [47] M. Szewc, E.B. Radzikowska, P. Wdowiak, J. Kozak, P. Kusza, E. Niezabitowska, M. Maslyk, MSCs as tumor-specific vectors for the delivery of anticancer agents—a potential therapeutic strategy in cancer diseases: perspectives for quinazolinone derivatives, *Int. J. Mol. Sci.* 23 (5) (2022) 2745, <https://doi.org/10.3390/ijms23052745>.
- [48] M.H.E. Shershaby, A. Ghiaty, A.H. Bayoumi, A.A.A. Karmalawy, E.M. Husseiny, M.S.E. Zoghbi, H.S. Abulkhair, From triazolo phthalazines to triazolo quinazolines: a bioisosterism-guided approach toward the identification of novel PCAF inhibitors with potential anticancer activity, *Bioorg. Med. Chem.* 42 (2021) 116266, <https://doi.org/10.1016/j.bmc.2021.116266>.
- [49] A.k. Mahato, B. Srivastava, S. Nithya, Chemistry, structure activity relationship and biological activity of quinazolin-4 (3H)-one derivatives, *InVentiv Rapid Med Chem* 2 (1) (2011) 13–19.
- [50] M. Dvorakova, L. Langhansova, V. Temml, A. Pavicic, T. Vanek, P. Landa, (Synthesis, inhibitory activity, and in silico modeling of selective COX-1 inhibitors with a Quinazolinone core, *ACS Med. Chem. Lett.* 12 (4) (2021) 610–616, <https://doi.org/10.1021/acs.medchemlett.1c00004>.
- [51] H. Li, Q. Yang, M. Su, F. Luo, Y. Liu, D. Wang, Y. Fan, design, synthesis, and biological evaluation of novel 6-(pyridin-3-yl) quinazolin-4 (3H)-one derivatives as potential anticancer agents via PI3K inhibition, *Bioorg. Med. Chem.* 46 (2021) 116346, <https://doi.org/10.1016/j.bmc.2021.116346>.
- [52] S.K. Muthuvel, E. Elumalai, K. Girija, K. Hemalatha, Molecular docking and dynamics studies of 4- anilino quinazolines for epidermal growth factor receptor tyrosine kinase to find potent inhibitor 38 (2019) 475–483, <https://doi.org/10.1080/10799893.2019.1590411>.
- [53] W. Dohle, F.L. Jourdan, G. Menchon, A.E. Prota, P.A. Foster, P. Mannion, E. Hamel, M.P. Thomas, P.G. Kasprzyk, E. Ferrandis, M.O. Steinmetz, M.P. Leese, B.V. L. Potter, Quinazolinone-based anticancer agents: synthesis, antiproliferative SAR, antitubulin activity, and tubulin Co-crystal structure, *J. Med. Chem.* 61 (3) (2018) 1031–1044, <https://doi.org/10.1021/acs.jmedchem.7b01474>.
- [54] P.M. Quan, L.T.T. Huong, P.T.H. Minh, T.Q. Toan, D.T. Lam, V.T.T. Le, P.Q. Long, Review: auto dock 4.2.6 as an effective tool for molecular docking studies against SARS-cov-2 main protease: a tutorial using mgl tools, *Vietnam Journal of Science and Technology* 60 (6) (2022) 929–947, <https://doi.org/10.15625/2525-2518/16459>.
- [55] J. Stamos, M.X. Sliwkowski, C. Eigenbrot, Structure of the epidermal growth factor receptor kinase domain alone and in complex with a 4-anilinoquinazolinone inhibitor, *J. Biol. Chem.* 277 (48) (2002) 46265–46272.
- [56] A. Sonousi, R.A. Hassan, E.O. Osman, A.M. Abdou, S.H. Emam, Design and synthesis of novel quinazolinone-based derivatives as EGFR inhibitors with antitumor activity, *J. Enzym. Inhib. Med. Chem.* 37 (1) (2022) 2644–2659, <https://doi.org/10.1080/14756366.2022.2118735>.
- [57] S. Keretsu, S. Ghosh, S.J. Cho, Molecular modeling study of c- ki T/PDGF α dual inhibitors for the treatment of gastrointestinal stromal tumors, *Int. J. Mol. Sci.* 21 (21) (2020) 8232.
- [58] M.F. Adasme, K.L. Linnemann, S.N. Bolz, F. Kaiser, S. Salentin, V.J. Haupt, M. Schroeder, Plip 2021: expanding the scope of the protein–ligand interaction profiler to DNA and RNA, *Nucleic acids research* 49 (W1) (2021) W530–W534, <https://doi.org/10.1093/nar/gkab294>.
- [59] C.C. Wu, T.K. Li, L. Farh, L.Y. Lin, T.S. Lin, Y.J. Yu, T.J. Yen, C.W. Chiang, N.L. Chan, Structural basis of type II topoisomerase inhibition by the anticancer drug etoposide, *Science* 333 (2011) 459–462, <https://doi.org/10.1126/science.1204117>.
- [60] C.A. Lipinski, Lead- and drug-like compounds: the rule-of-five revolution, *Drug Discov. Today Technol.* 1 (2004) 337–341.
- [61] K. Sangphreak, M. Mueller, N. Darai, P. Wolschann, C. Suwattanasophon, R. Ruga, W. Chavasiri, S. Seetaha, K. Choowongkamon, N. Kungwan, C. Rungnim, C. J. Enzyme, Computational screening of chalcones acting against topoisomerase II α and their cytotoxicity towards cancer cell lines, *Inhibit Med Chem* 34 (1) (2019) 134–143, <https://doi.org/10.1080/14756366.2018.1507029>.
- [62] P. Panyada, N. Nunthaboot, P. Puthongking, In silico ADME, metabolism prediction and hydrolysis study of melatonin derivatives, *Int. J. Tryptophan Res.* 13 (2020) 1178646920978245, <https://doi.org/10.1177/1178646920978245>.
- [63] A. Daina, O. Michielin, V. Zoete, Swiss ADME: a free web tool to evaluate phar microkinetic, drug-likeness and medicinal chemistry friendliness of small molecules, *Sci. Rep.* 7 (2017) 42717, <https://doi.org/10.1038/srep42717>.
- [64] Y. Bai, H. Sui, X. Liu, L. He, X. Li, E. Thormann, Effects of the N, O, and S heteroatoms on the adsorption and desorption of asphaltene on silica surface: a molecular dynamics simulation, *Fuel* 240 (2019) 252–261, <https://doi.org/10.1016/j.fuel.2018.11.135>.

- [65] R.A. Dabhi, M.P. Dhaduk, V.D. Bhatt, B.S. Bhatt, Synthetic approach toward spiro quinoxaline- β -lactam based heterocyclic compounds: spectral characterization, SAR, pharmacokinetic and biomolecular interaction studies, *J. Biomol. Struct. Dyn.* 41 (12) (2023) 5382–5398, <https://doi.org/10.1080/07391102.2022.2086176>.
- [66] T. Dutta, A.P. Chattopadhyay, N.N. Ghosh, S. Khatua, K. Acharya, S. Kundu, D. Mitra, M. Das, Biogenic silver nanoparticle synthesis and stabilization for apoptotic activity; insights from experimental and theoretical studies, *Chem. Pap.* 74 (2020) 4089–4101, <https://doi.org/10.1007/s11696-020-01216-z>.
- [67] Y.H. Zhao, M.H. Abraham, J. Le, A. Hersey, C.N. Luscombe, G. Beck, B. Sherborne, I/Cooper, Rate-limited steps of human oral absorption and QSAR studies, *Pharm. Res. (N. Y.)* 19 (10) (2002) 1446–1457, <https://doi.org/10.1023/a:1020444330011>.
- [68] N. Homeyer, H. Gohlke, Free energy calculations by the molecular mechanics Poisson–Boltzmann surface Area method, *Molecular Informatics* 31 (2) (2012) 114–122, <https://doi.org/10.1002/minf.201100135>.
- [69] A.W. Gotz, M.J. Williamson, D. Xu, D. Poole, S.L. Grand, R.C. Walker, Routine microsecond molecular dynamics simulations with AMBER on GPUs. 1. Generalized born, *J. Chem. Theor. Comput.* 8 (5) (2012) 1542–1555, <https://doi.org/10.1021/ct200909j>.
- [70] M. Strong, M.R. Sawaya, S. Wang, M. Phillips, D. Cascio, D. Eisenberg, Toward the structural genomics of complexes: crystal structure of a PE/PPE protein complex from *Mycobacterium tuberculosis*, in: *Proceedings of the National Academy of Sciences*, vol. 103, 2006, pp. 8060–8065, <https://doi.org/10.1073/pnas.0602606103>, 21.
- [71] R.A. Krishnan, A. Drozdetski, R.C. Walker, A.V. Onufriev, Speed of conformational change: comparing explicit and implicit solvent molecular dynamics simulations, *Biophys. J.* 108 (5) (2015) 1153–1164, <https://doi.org/10.1016/j.bpj.2014.12.047>.
- [72] A. Godfrey, R. Conway, D. Meagher, G. O’laighin, Direct measurement of human movement by accelerometry, *Med. Eng. Phys.* 30 (10) (2008) 1364–1386, <https://doi.org/10.1016/j.medengphy.2008.09.005>.
- [73] R.S. Ferrer, A.W. Gotz, D. Poole, S. Le Grand, R.C. Walker, Routine microsecond molecular dynamics simulations with AMBER on GPUs. 2. Explicit solvent particle mesh Ewald, *J. Chem. Theor. Comput.* 9 (9) (2013) 3878–3888, <https://doi.org/10.1021/ct400314y>.
- [74] T. Darden, D. York, L. Pedersen, Particle mesh Ewald: an $N \cdot \log(N)$ method for Ewald sums in large systems, *J. Chem. Phys.* 98 (12) (1993) 10089–10092, <https://doi.org/10.1063/1.464397>.
- [75] W.L. Jorgensen, J. Chandrasekhar, J.D. Madura, R.W. Impey, M.L. Klein, Comparison of simple potential functions for simulating liquid water, *J. Chem. Phys.* 79 (2) (1983) 926–935, <https://doi.org/10.1063/1.445869>.
- [76] H. worth, A. Scott, R.O. Dror, Molecular dynamics simulation for all, *Neuron* 99 (6) (2018) 1129–1143, <https://doi.org/10.1016/j.neuron.2018.08.011>.
- [77] B.C. Jacobs, B. van den Berg, C. Verboon, G. Chavada, D.R. Cornblath, K.C. Gorson, C. Nascimbene, International Guillain-Barré Syndrome Outcome Study: protocol of a prospective observational cohort study on clinical and biological predictors of disease course and outcome in Guillain-Barré syndrome, *J. Peripher. Nerv. Syst.* 22 (2) (2017) 68–76, <https://doi.org/10.1111/jns.12209>.
- [78] R.B.J.S. Krishnan, J.S. Binkley, R. Seeger, J.A. Pople, Self-consistent molecular orbital methods. XX. A basis set for correlated wave functions, *J. Chem. Phys.* 72 (1) (1980) 650–654, <https://doi.org/10.1063/1.438955>.
- [79] T. Clark, J. Chandrasekhar, G.W. Spitznagel, P.V.R. Schleyer, Efficient diffuse function-augmented basis sets for anion calculations. III. The 3-21+ G basis set for first-row elements, Li–F, *J. Comput. Chem.* 4 (3) (1983) 294–301, <https://doi.org/10.1002/jcc.540040303>.